VCP/p97 regulates Beclin-1-dependent autophagy initiation

Sandra M. Hill[1,2,4], Lidia Wrobel[1,4], Avraham Ashkenazi[1,4,#], Marian Fernandez-Estevez[1,4], Keith Tan[3], Roland W. Bürli[3], David C. Rubinsztein[1,4,*]

[1] Department of Medical Genetics, Cambridge Institute for Medical Research, The Keith Peters Building, Cambridge Biomedical Campus, Hills Road, Cambridge CB2 0XY, United Kingdom

[2] Department of Psychiatry and Neurochemistry, Institute of Neuroscience and Physiology, The Sahlgrenska Academy at the University of Gothenburg, 413 45 Gothenburg, Sweden

[3] Neuroscience, BioPharmaceuticals R&D, AstraZeneca Cambridge, CB21 6GH, UK, Cambridge, UK

[4] UK Dementia Research Institute, University of Cambridge, Cambridge Institute for Medical Research, The Keith Peters Building, Cambridge Biomedical Campus, Hills Road, Cambridge CB2 0XY, United Kingdom

[#] Current address: Faculty of Medicine, Sagol School of Neuroscience, Tel Aviv University, 6997801, Tel Aviv, Israel.

* Lead contact and correspondence: dcr1000@cam.ac.uk

Abstract

Autophagy is an essential cellular process that removes harmful protein species, and autophagy upregulation may be able to protect against neurodegeneration and various pathogens. Here, we have identified the essential protein VCP/p97 as a novel regulator of autophagosome biogenesis, where VCP regulates autophagy induction in two ways, both dependent on Beclin-1. Utilizing small-molecule inhibitors of VCP ATPase activity, we show that VCP stabilizes Beclin-1 levels by promoting the deubiquitinase activity of Ataxin-3 towards Beclin-1. VCP also regulates the assembly and activity of the Beclin-1-containing phosphatidylinositol-3-kinase (PI3K) complex I, thus regulating the production of PI(3)P, a key signaling lipid responsible for the recruitment of downstream autophagy factors. Decreased levels of VCP, or inhibition of its ATPase activity impairs starvation-induced production of PI(3)P and

limits downstream recruitment of WIPI2, ATG16L and LC3, thereby decreasing autophagosome formation, illustrating an important role for VCP in early autophagy initiation.

Keywords

Autophagy, VCP, Beclin-1, Ataxin-3, Neurodegeneration

Introduction

Macroautophagy (henceforth autophagy) is an essential cellular process for degradation and recycling of cytosolic material, including entire organelles. These substrates are engulfed by double-membrane cup-shaped structures called phagophores. After the edges of the phagophores close, they become known as autophagosomes, which ultimately fuse to lysosomes to enable their degradation. Autophagy protects against the accumulation of damaged and dysfunctional components. The ability to upregulate autophagy is desirable from a therapeutic perspective as it protects against several metabolic and neurodegenerative diseases, as well as against cancer initiation [1].

During autophagy induction, the sites of phagophore formation are determined by a confined enrichment of the lipid phosphatidyinositol-3-phosphate (PI(3)P) on precursor membranes [2-4]. The PI(3)P is produced by the phosphatidyinositol-3-kinase (PI3K) complex I, consisting of the kinase VPS34 together with the regulatory proteins VPS15, Beclin-1 and ATG14L. Many upstream signaling pathways converge to regulate this kinase complex and the levels of its components in order to modulate autophagy [5]. PI3K kinase activity results in the recruitment of PI(3)P-binding proteins, which eventually mediate the conjugation of ATG8 family proteins, such as LC3, to phosphatidylethanolamine in phagophore membranes [6,7]. Lipid-conjugated LC3 levels (LC3-II) correlate with autophagic load and LC3-II levels in the presence of lysosomal inhibitors (like Bafilomycin A1) reflect rates of LC3-II/autophagosome formation [8].

Here we have identified Valosin-containing protein (VCP, also called p97), an essential and evolutionary conserved ATPase associated with diverse cellular activities [9], as a novel regulator of autophagy initiation. Our findings are distinct from previous studies that have observed that cells expressing dysfunctional versions of

VCP accumulate immature autophagic vesicles, positive for LC3 and p62 [10-12], and display defects in autophagic clearance [13-16], indicative of a role in autophagosome maturation and fusion with the lysosome.

The role of VCP in autophagosome maturation has been attributed to VCP affecting multiple steps of endocytosis. This may affect autophagic flux, as autophagosome-endosome fusion precedes autophagosome-lysosome fusion [17]. VCP interacts with the endocytic coat protein Clathrin, and regulate caveolin trafficking through the endosomal system [15,18]. Furthermore, VCP has been suggested to regulate the oligomeric assembly of EEA1 oligomers, thereby governing the size and trafficking rate of early endosomes [14]. In addition, VCP has been implicated in the autophagic removal of lysosomes themselves (lysophagy) [13], by modulating ubiquitin linkages on damaged lysosomes to enable LC3 binding and recruitment to autophagosomes. Thus, the mechanisms for VCP regulation of autophagosome maturation involves both endosomal transport as well as maintenance of a healthy pool of lysosomes.

Here, we exploit the ability to acutely inhibit VCP activity with small-molecule inhibitors to show that VCP regulates autophagy induction and the formation of autophagosomes, in addition to regulating autophagosome maturation. We identify VCP as a novel interactor of the key autophagy protein Beclin-1 and show that VCP stimulates Ataxin-3-dependent stabilization of Beclin-1 levels. In addition, VCP acts to enhance the assembly and activity of the Beclin-1-containing PI3K complex in a manner independent of Ataxin-3. Through these two mechanisms, VCP stimulates the production of PI(3)P, and governs the recruitment of early autophagosome markers, thereby fulfilling an important role in early initiation of autophagy.

Results

VCP interacts with Beclin-1 and affects autophagy

PI(3)P formation in autophagy initiation is Beclin-1-dependent, and we have previously shown that Ataxin-3 interacts with Beclin-1 and regulates the levels of this protein, thereby influencing autophagy[19]. Other studies have showed that Ataxin-3 interacts with the major ATPase VCP [20-23], and we thus hypothesized that VCP could interact with Beclin-1, directly or indirectly, and possibly play a role in Beclin-1 dependent autophagy. We could indeed verify the endogenous interaction of these two proteins in human cells (Fig. 1a), where VCP co-immunoprecipitated with Beclin-1. To gain mechanistic insights into the interaction between VCP and Beclin-1 we attempted to map the binding site using truncated versions of Beclin-1 [24]. While we were able to confirm the interaction between VCP and full-length Beclin-1 *in vitro*, we could not pinpoint a specific region of Beclin-1 responsible for VCP binding, as VCP was found to bind all of the different truncated proteins of Beclin-1 (Extended Data Fig. 1a-c). While this could indicate that VCP is able to interact with Beclin-1 at several sites, this could also be a consequence of improper folding of the Beclin-1 truncations leading to recognition by the chaperone-like activity of VCP [25].

The interaction between the two proteins both *in vivo* and *in vitro* prompted us to test if VCP regulated Beclin-1-dependent autophagosome biogenesis. This would represent a new role for VCP in autophagy initiation, in addition to its reported functions in autophagosome maturation/clearance [10-12]. In order to distinguish between effects on autophagosome formation and degradation, we acutely inhibited VCP activity with the reversible inhibitor DBeQ and combined this with pre-treatment using Bafilomycin A1 (BafA) to impair lysosome activity, which allowed us to assess LC3-II/autophagosome formation. In both basal and starvation conditions (where autophagy is induced), DBeQ caused an accumulation of LC3-II in the absence of BafA, but a decrease in LC3-II levels in the presence of BafA, corresponding to a combined phenotype where both autophagosome formation and degradation are impaired (Fig. 1b-c). The impaired starvation response upon VCP inhibition with DBeQ could be recapitulated in mouse primary cortical neurons (Extended Data Fig. 1d), and was further demonstrated by the absence of starvation-induced LC3 puncta in cells (Fig. 1d-e). Inhibition of the starvation response was further recapitulated using additional commercial VCP inhibitors, where both the allosteric inhibitor NMS873 [26], and the competitive DBeQ analogue CB-5083 [27] impaired the increase of LC3 puncta (autophagosome numbers) upon starvation (Extended Data Fig. 2a-c).

The loss of LC3 induction upon VCP inhibition was accompanied with a reduction in the production of PI(3)P by the Beclin-1-containing PI3K complex, which is an early signal for autophagy induction that acts upstream of LC3 recruitment to autophagosomes [5]. We found that starvation-induced PI(3)P production was impaired upon acute VCP inhibition with DBeQ (Fig. 1f and Extended data figure 2d) as well as with the VCP inhibitors NMS873 and CB-5083 (Extended Data Fig. 2e-g). The extent of reduction in starvation-induced PI3K activity for VCP inhibition was in the same range as following direct PI3K kinase inhibition by Wortmannin or IN1 (Fig.1f and Extended Data Fig. 2d-g), indicating a strong dependence of VCP activity for PI(3)P production. Additionally, *VCP* knockdown impaired ATG5-12 conjugation, an early step preceding LC3-II formation which is Beclin-1/PI(3)P-dependent [28], further supporting a role for VCP in autophagy initiation (Extended data Fig. 2h).

While loss of PI(3)P induction upon starvation could be seen also upon siRNA-mediated knockdown of *VCP* (Extended Data Fig. 3a-b), the defect in LC3-II (autophagosome formation) production seen with VCP inhibitors could not be replicated using this genetic knockdown approach (Extended Data Fig 3c-d), possibly due to the long-term accumulation of autophagosomes masking any visible effects on formation enabled by 4 h BafA treatment at the end of the experiment, or secondary effects arising during the prolonged depletion of an essential protein. Indeed, we observed that knockdown of *VCP* even using low concentrations of siRNA resulted in growth arrest and a large proportion of cell death (not shown), in agreement with previously published studies [29,30]. Thus, the acute inhibition of VCP using available inhibitors provides us with a tool for studying its role in essential cellular processes, while avoiding the detrimental effects of *VCP* knockdown.

VCP governs the recruitment of early autophagy markers

To further focus on the effects on VCP on early autophagy initiation, we studied the appearance of early autophagy markers, which, unlike LC3 levels, would be unaffected by a potential block in autophagosome fusion to the lysosome, thus allowing us to discriminate between the role of VCP in autophagy induction versus its role in autophagosome maturation. WD repeat domain phosphoinositide-interacting protein 2 (WIPI2) is recruited to sites of autophagy initiation by binding to PI(3)P and, in turn, recruits the ATG12-ATG5-ATG16L complex to enable downstream recruitment and conjugation of LC3 to the forming autophagosome membranes [31].

We found that inhibition of VCP with DBeQ significantly impaired starvation-induced accumulation of both WIPI2 (Fig. 2a-b) and ATG16L puncta (Fig 2c-d), as would be expected after the decreased production of PI(3)P. The same effect was seen using additional VCP inhibitors NMS873 and CB-5083 (Extended Data Fig. 4a-b and 4d-e). In addition to the observed impairment of starvation-induced autophagy, we also found LC3 puncta accumulation upon treatment with the mTOR inhibitor, Torin 1 (which recapitulates the mTORC1 inhibition component of starvation-induced autophagy), to be abolished by VCP inhibition (Extended Data Fig 4c and 4f). Thus, VCP interacts with Beclin-1 and is important for PI(3)P production by the Beclin-1-containing PI3K complex during multiple scenarios of autophagy induction.

VCP stabilizes Beclin-1 levels via Ataxin-3

Genetic knockdown of *VCP* expression or inhibition of VCP activity reduced Beclin-1 protein levels in both primary mouse neurons and in human cells (Fig. 3a, and Extended Data Fig. 5a-b). VCP inhibition with DBeQ also reduced Beclin-1 levels in the presence of the translational inhibitor cycloheximide (CHX), which was blocked by the addition of the proteasome inhibitor MG132, suggesting that VCP inhibition caused more rapid proteasomal degradation of Beclin-1 (Fig. 3b). Thus, loss of VCP function leads to destabilization of Beclin-1 and a decreased production of PI(3)P and LC3-II, compromising autophagy induction.

We have previously reported that the deubiquitinase Ataxin-3 stabilizes Beclin-1, and that loss of Ataxin-3 reduces Beclin-1 levels and impairs autophagosome biogenesis [19]. VCP has been reported to bind Ataxin-3 and to stimulate its deubiquitinase activity towards synthetic substrates *in vitro* [20-23], and Ataxin-3 together with VCP are important for nematode survival during pro-longed starvation[32]. Hence, Ataxin-3-dependent stabilization of Beclin-1 encompasses a potential mechanism to explain the role of VCP in autophagy initiation. We found that knockdown and inhibition of VCP decreased levels of both Ataxin-3 and Beclin-1 (Fig. 3a-b, Fig. 3c; input, and Extended Data Fig. 5a-c) and postulated that a drop in protective deubiquitination by Ataxin-3 destabilized Beclin-1 in VCP-inhibited cells. To investigate the role of VCP in Ataxin-3-dependent regulation of Beclin-1, we utilized an Ataxin-3 mutant with compromised binding ability to VCP (Ataxin-$3_{\Delta VCP}$; Extended Data Fig. 5d) [33]. While the interaction between Ataxin-3 and Beclin-1 is not dependent on VCP (Fig. 3c and Extended Data Fig. 5e), the binding of Ataxin-3 to VCP seems to increase the ability of Ataxin-3 to protect Beclin-1 from proteasomal degradation, as overexpression of Ataxin$3_{\Delta VCP}$ was less able to stabilize Beclin-1 levels compared to overexpression of

the wildtype Ataxin-3 allele (Fig. 3d-e). These effects are likely proteasome-dependent, as no significant differences were observed between these constructs in cells treated with the proteasome inhibitor, MG132 (Fig. 3d-e). Similarly, rescue of LC3 puncta formation (autophagosome numbers) in *ATAXIN-3* knockdown cells was more efficiently accomplished by wild-type Ataxin-3, compared to Ataxin3$_{\Delta VCP}$ (Fig. 3f and Extended Data Fig. 6a-b). Furthermore, we could show that in the presence of ATP, VCP stimulates Ataxin-3 deubiquitination of Beclin-1 *in vitro* (Fig. 3g and Extended Data Fig. 6c). A significant decrease in Beclin-1 ubiquitination was observed when VCP or Ataxin-3 were added alone (Fig. 3g), but the combination of the two proteins yielded an even more pronounced reduction in Beclin-1 ubiquitination, hence providing evidence for VCP regulation of Ataxin-3 deubiquitination towards a physiologically relevant substrate. Together, these data indicate that VCP binding of Ataxin-3 is important to protect Beclin-1 from proteasomal degradation, by stimulating the deubiquitinase activity of Ataxin-3 towards Beclin-1. Thus, stabilization of Beclin-1 via Ataxin-3 provides one possible mechanism for VCP-dependent regulation of autophagosome formation.

VCP interacts with PI3K complex

Beclin-1 is a core component of the PI3K complex, which exists in at least three different compositions to regulate autophagy at different steps, and endocytosis [34]. The core components VPS15, VPS34 and Beclin-1 form PI3K complex I together with ATG14L to regulate autophagosome formation, while in complex II ATG14L is replaced by UVRAG to positively regulate endocytosis [35,36]. In complex III, Rubicon binds UVRAG to negatively regulate the activity of the complex [37,38]. We found that endogenous VCP interacts with all three PI3K complexes (Fig. 4a), as it could be identified in immunoprecipitations of endogenous ATG14L, UVRAG as well as Rubicon. We therefore focused further studies on the ATG14L-containing complex I to gain insights into the role of VCP in autophagosome formation. VCP interacted with ATG14L even in cells where expression of *ATAXIN-3* or *BECLIN-1* had been reduced by siRNA-mediated knockdown (Fig. 4b-c), and Ataxin-3 was found associated with the ATG14L-containing PI3K complex even when Beclin-1 levels were diminished (Fig. 4d). Thus, we considered roles for VCP in PI3K complex I assembly, as a distinct role from its ability to stabilize Beclin-1 levels.

Knockdown of *VCP* reduced the amount of total ATG14L as well as the amount of ATG14L associated with Ataxin-3 (Extended Data Fig. 7a). The reduced levels of ATG14L could be an indirect effect of decreased Beclin-1 levels, as the PI3K

complex members are known to stabilize each other [38,39]. Thus, while our previous data showed no effect on the Ataxin-3 and Beclin-1 interaction upon VCP inhibition (Fig. 3c), VCP might enhance the recruitment of Ataxin-3 to the pool of Beclin-1 in complex with ATG14L. The interaction of VCP with the PI3K complex I seems independent of Ataxin-3 and Beclin-1, suggesting that VCP can interact with additional components of the PI3K complex. In agreement with this, we found that VCP interacts directly with VPS34, ATG14L and Beclin-1 of the PI3K complex I *in vitro* (Extended Data Fig. 7b-d; VPS15 was not included as it could not be individually purified), further indicating that VCP could interact with the PI3K complex in the absence of Ataxin-3. A mutated version of the VCP cofactor UFD1L, $UFD1L_{\Delta VCP}$ (Δaa215-241; [40]), was used as a negative control in binding experiments.

VCP regulates PI3K assembly *in vitro* and *in vivo*

Addition of VCP to pre-assembled PI3K complexes (Extended Data Fig. 8a) increased the *in vitro* production of PI(3)P (Fig. 4e), suggesting that we should test if VCP facilitates the assembly of the PI3K complex itself, in addition to bringing Ataxin-3 close to Beclin-1. In agreement with a role for VCP in regulating PI3K assembly, knockdown of *VCP* expression decreased the interaction between ATG14L (as a surrogate for PI3K complex I) with the PI3K components Beclin-1 and VPS34 (Extended data Fig. 8b-c). Similarly, inhibition of VCP ATPase activity also interfered with the interaction of ATG14L with the PI3K components VPS15, VPS34 and Beclin-1 (Fig. 5a-b), as well as with the binding of VCP itself to ATG14L, indicating that the presence and activity of VCP is aiding PI3K assembly. When analyzing the amount of VCP pulled down by endogenous ATG14L after VCP inhibition, we detected two bands for VCP: one around 100 kDa as expected for endogenous VCP and one band slightly above. This band may be a post-translationally modified version of VCP that is enriched in the interaction with PI3K, and since it could be detected also in the input (Extended data Fig. 8d, long exposure) and was affected by siRNA against VCP (Extended data Fig. 8e), both VCP bands were included in quantifications. Of the VCP inhibitors used, CB-5083 was the only inhibitor that did not cause a clear trend of decreased interactions of PI3K complex I components with ATG14L (Fig. 5a-b), perhaps related to it only inhibiting the D2 ATPase activity of VCP, whereas the other inhibitors affect both ATPase domains [41,42].

We further demonstrated that VCP directly acts to enhance the assembly of individually purified components into complete PI3K complexes *in vitro*, as co-purification with ATG14L was increased for all the PI3K components when VCP was

present (Fig 5c-d, Extended data Fig. 8f). Thus, the binding of VCP to PI3K components enhances the assembly of fully formed complexes in a manner that requires VCP ATPase activity.

Discussion

In this study, we identify two unforeseen functions for VCP in autophagy initiation. First, VCP binds both Ataxin-3 and Beclin-1 in the PI3K complex, thereby enhancing the deubiquitination and stabilization of Beclin-1 (Fig. 5e; left). Thus, inhibition or knockdown of VCP decreases levels of Beclin-1 and inhibits autophagy. Second, VCP interacts with multiple components of the Beclin-1-containing PI3K complex and enhances complex assembly and resultant kinase activity, increasing the production of the autophagy signaling lipid PI(3)P (Fig. 5e; right). Inhibition of VCP ATPase activity blocks both functions, indicating that both roles of VCP require ATP hydrolysis. As VCP interacts in a binary fashion with the components of the complex, it may be simply acting as a scaffold to enhance complex formation. It is possible that this process may be driven by ATP-dependent conformational changes (as it is blocked by VCP inhibitors), or by bridging the kinase and substrate contact, as VCP have been suggested to bind lipids such as phosphoinositols [43,44].

The link between VCP and Ataxin-3 activity had been previously established *in vitro* [23], and the two proteins have been implicated in promoting autophagy where Ataxin-3 was found also to interact with the autophagosome protein LC3 [32]. While our data provides a link between these two findings, and show that VCP and Ataxin-3 acts to stimulate Beclin-1 levels to promote autophagy, it remains to be determined whether VCP also influences the proposed interaction between Ataxin-3 and LC3 and if this is yet another mechanism whereby VCP could influence autophagy initiation.

Studies on the role of VCP in autophagy have thus far been focused on its role in autophagosome maturation, as the defect in autophagosome formation is masked by the strong maturation phenotype seen when reducing VCP levels or activity. We overcame this issue by combining an initial inhibition of lysosome fusion with a subsequent acute inhibition of VCP activity using three different VCP specific inhibitors (DBeQ, NMS873 and CB-5083) to detect a decrease in autophagosome marker LC3. Initial disruption of lysosomal fusion before addition of VCP inhibitors was crucial to avoid the consequences of VCP inhibition on lysosomal function. With simultaneous administration of lysosome and VCP inhibitors, VCP inhibitors could

exert their function on autophagosome maturation before lysosomal inactivation occurred, thus leading to an accumulation of LC3-positive autophagosomes [16].

Utilizing chemical VCP inhibitors, we were further able to see a decrease in PI(3)P production and the subsequently reduced recruitment of early autophagy markers. Thus, the acute inhibition of VCP provided us with a tool to characterize a role for VCP in autophagy initiation which had previously gone unrecognized in genetic knockdown experiments. The use of inhibitors also allows one to readily assess if effects are simply due to inert protein or due to its ATPase activity. Our proposed model for VCP regulating PI(3)P production could potentially comprise an additional mechanism for the block in autophagosome maturation seen upon reduced VCP activity. As PI(3)P also plays an important role in endosomal membrane fusion and endocytic trafficking [45], it provides a possible mechanism whereby VCP activity could influence both autophagy initiation and maturation.

Mutations in the essential *VCP* gene have been linked to multisystem disorders including Inclusion body myopathy with early-onset Paget disease and frontotemporal dementia (IBMPFD) and neurogenerative diseases such as Parkinson's disease and Amyotrophic lateral sclerosis (ALS) [10,46,47]. It is possible that the different aspects of these disorders are linked to the diverse functions of VCP, and that some could be explained by a decreased ability for autophagy induction as described by our data. For instance, mutations in VCP affecting ATPase activity has been linked to an increased abundance of pathologic tau fibrils and the development of frontotemporal degeneration [48], and while this could be an effect of impaired disaggregase activity of VCP [49] it Is also feasible that the accumulation of tau could be due to a decline in VCP-dependent autophagic capacity, since tau is an autophagy substrate.

It remains to be determined how the temporal and local recruitment of VCP to PI3K is regulated. Our observation that VCP co-purified with ATG14L runs as two bands on a western blot indicates the possibility of posttranslational regulation of VCP. ULK1 and ULK2 are two upstream kinases known to regulate autophagy that phosphorylate VCP to regulate the disassembly of heat-induced stress-granules [50], and thus encompass potential candidates for upstream regulation, although this needs to be further investigated in future studies. Furthermore, it remains to be elucidated which (if any) of the known VCP cofactors are important for this proposed role in autophagosome formation.

In conclusion, our findings add to the complexity of the cellular functions of VCP and provides evidence for its role as an important regulator of autophagy initiation.

Online Methods

EXPERIMENTAL MODELS

Cell Lines

Human cervical epithelium HeLa (ATCC; #CCL-2; CVCL_0030), and human embryonic kidney cell line HEK293 (ECACC; #85120602) were cultured in Dulbecco's modified Eagle's medium (DMEM) (4.5 mg/L of glucose; Sigma) supplemented with 10% FBS (Sigma), 2mM L- glutamine (Sigma) and 100 U/mL penicillin and 100 mg/mL streptomycin (Sigma). Human embryonic suspension cells, Expi293F (Gibco; #A14527), were grown in Expi293 Expression Medium (Gibco)

All cell lines were maintained at 37℃ and 5% CO_2 and were regularly tested for mycoplasma contamination. All cell lines are of female origin (HeLa, HEK293, Expi293F). For starvation experiments using cell lines, cells were washed three times in starvation media (Hank's balanced salt solution (HBSS, Invitrogen) or Earle's balanced salt solution (EBSS, Sigma) and incubated for 2-4 h at 37°C.

Mouse primary neurons

All animal studies and procedures were performed with project licenses granted by the UK Home Office and with the approval of the University of Cambridge committee for animal studies. Primary cortical neurons were isolated from C57BL/6 mice (Jackson Laboratories) embryos of mixed sex at E16.5 as previously described [19]. Briefly, embryo brains were harvested and placed in PBS/glucose where the meninges were removed, and the cerebral cortices were dissected. After mechanical dissociation using sterile micropipette tips, dissociated neurons were resuspended in PBS+glucose and collected by centrifugation. Viable cells were seeded on poly-ornithine-coated 12-multiwell plates. Cells were cultured in Neurobasal medium (Thermo Fisher Scientific) supplemented with 2 mM glutamine, 200 mM B27 supplement and 1% Penicillin-Streptomycin at 37°C in a humidified incubator with 5% CO2. One half of the culture medium was changed every two days until

treatment/infection. After 5 days of *ex vivo* culturing, differentiated neurons were treated with different drugs.

METHODS DETAILS

Antibodies and Reagents

The following primary antibodies have been used in this work: mouse anti-Flag M2 (1:1000), and rabbit anti-Actin (RRID AB_476693; 1:1000) from Sigma Aldrich; rabbit anti-VCP (RRID: AB_259529; 1:2000), rabbit anti-LC3B (RRID: AB_10003146; 1:400 for IF), rabbit anti-GFP (RRID:AB_305564; 1:1000), mouse anti-GFP (RRID: AB_298911; 1:1000), rabbit anti-RUBICON (RRID: AB_2827795; 1:1000), rabbit anti-VPS15 (RRID: AB_11141464; 1:1000), Rabbit anti-VPS34 (RRID: AB_2827796; 1:1000), mouse-anti-GAPDH (RRID: AB_2107448; 1:1000), and mouse-anti-WIPI2 (RRID: AB_105459; 1:100 for IF) from Abcam; rabbit anti-LC3B (RRID: AB_10003146; 1:1000) from Novus Biologicals; mouse anti-Ataxin-3 (RRID: AB_2129339; 1:1000) from EMD Millipore; rabbit anti-Beclin-1 (RRID: AB_490837; 1:1000), rabbit anti-UVRAG (RRID: AB_2687988; 1:1000); rabbit anti-ATG12 (RRID: AB_2059086; 1:1000) and rabbit anti-ATG16 (RRID: 8089s 1:100 for IF) from Cell Signaling; rabbit anti-ATG14L (RRID: AB_1953054; 1:1000), mouse anti-ATG14L (RRID: AB_10897331; 1:1000) from MBL. VCP inhibitors in DMSO was added to cell culture media for denoted incubation times: DBeQ (Selleckchem) was used at 10 µM, NMS873 (Selleckchem) was used at 10 µM, and CB-5083 (Selleckchem) was used at 2 or 5 µM. The concentrations used in this study was based on previously established concentrations for cell culture demonstrating a measurable effect on VCP activity in various cellular functions [51-57].

DNA constructs

The following DNA constructs were used in this study: pCMV6-FLAG-Myc (PS100001) and pMyc-FLAG-UFD1L (RC202989) from Origene; p3XFLAG-Beclin-1 (#24388), p3XFLAG-Ataxin-3 (#22126), pUbiquitin-HA (#18712), pStrep-Strep-FLAG-VPS15 (#99326), and pStrep-Strep-FLAG-VPS34 (#99327), pFLAG-Beclin1 (FL) (#24388), pFLAG-Beclin1 (1-150) (#24389), pFLAG-Beclin1 (151-241) (#24390), pFLAG-Beclin1 -(151-241) (#24393), pFLAG-Beclin1 (1-242) (#24391), pFLAG-Beclin1 (243-450) (#24392). p3XFLAG-ATG14L was a gift from Zhenyu Yue and pGEX-VCP-GST was kindly shared by Rolf Schröder and Cristoph Clemen.

Transfection

Trans IT-2020 reagent (Mirus) was used for DNA transfection, while Lipofectamine 2000 (Invitrogen) was used for siRNA transfections, according to the manufacturer's instructions. For protein production in HEK293 cells, TransIT-293 (Mirus) was used according to the manufacturer's instruction. For protein production in suspension Expi293F cells, transfection was performed with Polyethylenimine (PEI), at a ratio of 3:1 PEI:DNA. After transfection, cells were maintained in full medium. For knockdown experiments, cells were transfected with either a single or double round of 50 nM siRNA (Dharmacon; smartpool siRNA or single oligos). In single transfections (*VCP* and *BECLIN-1* knockdown), cells were split 24-48 h after transfection, and harvested 3 days post transfection. For knockdown of *VCP* for immunofluorescence, cells were transfected with 25 nM siRNA in suspension and plated at low density directly onto coverslips, followed by treatment and imaging after 48 h. For double transfections (*ATAXIN-3* knockdown), cells were transfected on day 1 and day 3. Cells were split twice, once after each transfection, and harvested 5 days after first transfection.

Western Blot Analysis

Cells were lysed in Laemmli sample buffer and boiled for 10 min at 100°C, separated by SDS-PAGE, transferred to PVDF membranes and developed with primary and secondary antibodies. Primary antibodies were used with overnight incubation at 4°C, unless otherwise stated, and the secondary antibodies are used at a concentration of 1:2000 and incubated for 1 h at room temperature. For immunoprecipitation experiments, light-chain specific secondary antibodies were used at a 1:1000 dilution for 1 h at room temperature. Blots were developed using an ECL enhanced chemiluminescence detection kit (GE Healthcare), or with direct infrared fluorescence detection on an Odyssey Infrared Imaging System. Western blots in main Figures 1a-c. 1h, 3a, 3c-e, 4a-c, and figures in extended data 1e, 3c, 5a, 5d, 5g, 5a and 6f were developed with chemiluminescence, while the other blots were developed with fluorescence (LICOR Odyssey system). Densitometric analysis on the immunoblots was performed using IMAGE STUDIO Lite software, which enables quantitative analysis of blotting signals.

Mutagenesis

3X-FLAG-Ataxin-3 (addgene #22126) was used as a template to mutate the VCP binding site and generate Ataxin-$3_{\Delta VCP}$ (282-285 RKRR/ANAA). Mutagenesis was

performed using QuikChange Multi Site-Directed MutagenesisKit (Agilent) and primer SMH17: (5'-CTTACTTCAGAAGAGCTTGCGAATGCAGCAGAAGCCTACTTTGAAAAG-3') according to manufacturer's instructions. Myc-FLAG-UFD1L plasmid (Origene RC213180) was used as template to mutate the VCP binding site and generate UFD1L$_{\Delta VCP}$ (Δ215-241) using QuikChange Site-Directed Mutagenesis Kit (Agilent) and the following primers: Fw: 5'-GTAGAGCCCAGCCCCTCC-3'; Rev: 5'-GGCTTCACCTTCTGTCGACTC-3'. All constructs were verified by sequencing.

Immunofluorescence

Staining of PI(3)P was performed as described previously[58]. Briefly, cells on coverslips were fixed in 2% paraformaldehyde and permeabilized with 20 µM digitonin in buffer A (20 mM Pipes pH 6.8, 137 mM NaCl, 2.7 mM KCl). Cells were blocked with buffer A supplemented with 5% (v/v) FBS and 50 mM NH_4Cl. Mouse-anti-PI(3)P antibody (1:400; 1 h at room temperature) (Echelon) and secondary antibody (1:400; 30 min at room temperature) (goat-anti-mouse Alexa Fluor 555; Thermo Scientific) were applied in buffer A with 5% FBS. Cells underwent post-fixation for 5 min in 2% paraformaldehyde, followed by 2X washes in PBS containing 50 mM NH_4Cl, and 1X wash with water before being mounted on microscope slides with ProLong Gold Antifade Mountant with DAPI (Thermo Scientific). For imaging of LC3 puncta, cells were fixed in ice cold methanol for 5 min, blocked in 1% BSA at room temperature for 1 h, permeabilized with 0,5% Triton X-100 for 5 min, then incubated with rabbit-anti-LC3B (abcam) overnight, and with secondary goat-anti-rabbit Alexa Fluor 647 for 1 h at room temperature. Imaging was conducted with LSM880 Zeiss confocal with 63X oil-immersion lens. For WIPI2 and ATG16 staining, cells were fixed in paraformaldehyde 4% for 10 minutes and permeabilized with 0.2% Triton X-100 for 10 minutes, then incubated with rabbit-anti-ATG16 (Cell signaling) and mouse-anti-WIPI2 (Abcam) for 1 h at room temperature, and with secondary goat-anti-rabbit Alexa Fluor 647 and goat-anti-mouse Alexa Fluor 488 for 1 h at room temperature. Imaging was conducted with LSM710 Zeiss confocal with 63X oil-immersion lens.

Protein Purification

Purification of VCP-GST from *E. coli*: Expression vector was transformed into bacterial strain Rosetta BL21 (DE3) (Novagen) according to instructions from supplier. Cells from a 1 L culture were harvested after overnight induction of protein

expression with 0.2 mM IPTG at 18°C. Cell pellet was resuspended in 2XPBS containing protease inhibitors and lysed by incubation with 0.5 mg/mL lysozyme for 30 min on ice, followed by sonication. Lysate was clarified by ultracentrifugation (100 000xg for 15 min at 4°C), and incubated with 1 mL glutathione sepharose resin (Pierce) for 2 h at 4°C. Resin was washed in a gravity flow column: 5X in 2XPBS and 5X in 2XPBS containing 0,1% Triton X-100 and 1 mM ATP. Purified protein was either cross-linked to beads for *in vitro* binding assays or eluted from beads by cleaving GST-tag with PreScission Protease. For crosslinking, beads were washed 3X in 200 mM HEPES (pH 8.5), and incubated with crosslinking solution (20 mM dimethyl pimelimidate in 200 mM HEPES pH 8.5) in RT for 60 min. Reaction was stopped by incubating beads with 0.2 M ethanolamine-HCl (pH 8.2) for 60 min. Beads were washed 3X in washing buffer (150 mM NaCl, 200 mM Glycine-HCl pH 2.0) and stored in binding buffer (25 mM HEPES pH 7.25, 200 mM NaCl, 0.01% Triton X-100, and 5% Glycerol, 1 mM DTT) containing 0.05% sodium azide.

For removal of GST tag, beads were washed 5X with PreScission cleavage buffer (50 mM Tris pH 7.0, 150 mM NaCl, 1mM EDTA, 1mM DTT, Triton X-100 0,01%), and resuspended in 475 μL cleavage buffer. 25 μL of PreScission protease was added and lysate was incubated overnight at 4°C, followed by collection of supernatant containing purified VCP.

Purification of FLAG-tagged PI3K complexes from HEK293: 10 μg of each plasmid (pStrep-Strep-FLAG-VPS15, p-Strep-Strep-FLAG-VPS34, 3X-FLAG-ATG14L and 3XFLAG-Beclin-1) and 75 μl of TransIT-293 used to transfect HEK293 cells in one 14 cm^2 poly-D-lysine coated dish. Cells were lysed 3 days post transfection in 1 mL lysis buffer CelLytic M (Sigma). Clarified lysates were incubated with 100 μL of M2 FLAG agarose resin (50% slurry) at 4°C for 2 h. Beads were added to a gravity flow column and washed 1X with lysis buffer, 10X with TBS and eluted in 100 μL TBS with FLAG peptides (150ng/μL) at 4°C 2 h. For purification of individual PI3K components, cells were transfected with 30 μg of the individual expression plasmid and purified using the same procedure with an additional washing step with high salt TBS (0.8 M NaCl) to remove the other complex components.

Purification of FLAG-VPS15 and FLAG-VPS34 from suspension cells: Expi293F suspension cells were grown to $2,5x10^6$ cells/mL in 500 mL of Expi293 Expression Medium (Gibco). Cells were transfected with 0,9 mg of pStrep-Strep-FLAG-VPS15 (addgene #99326) and 0,6 mg pStrep-Strep-FLAG-VPS34 (addgene #99327) and 4.5 mg Polyethylenimine 40K (Polysciences, Inc). On the day after transfection,

culture was expanded to 1 L, and 3.3 mM valproic acid (Sigma) and 10 mg/mL Penicillin/Streptomycin (Sigma) was added. Cells were lysed 3 days post transfection by homogenization in 50 mL Buffer A (50 mM HEPES pH 7.5; 200 mM NaCl; 5% glycerol; protease inhibitors) with 0.1 % CHAPS. Lysates were clarified by centrifugation at 100 000xg and incubated with 1,5 mL packed agarose M2 anti-FLAG resin (Sigma) for 2 h at 4°C. Resin was washed 3X with Buffer A, 3X with Buffer A with higher salt concentration (800 mM), and additional 4X in buffer A (200 mM NaCl). Proteins were eluted in fractions by incubation (4x60 min) with buffer A containing 150 ng/μl 3XFLAG peptides (Sigma). Purified proteins were analyzed on gel together with BSA standard to determine protein concentration.

Immunoprecipitation (IP)

For immunoprecipitation of endogenous proteins, cells from one 14 cm^2 dish were lysed in 0,2 mL of IP buffer (20 mM Tris pH 7.4; 2 mM $MgCl_2$; 200 mM NaCl; protease inhibitors) with 0,5% NP40, cleared by centrifugation, diluted to 1 mL by addition of IP lysis buffer (final 0,1% NP40). Lysates were pre-cleared for 1 h by incubation with non-targeting IgG control antibody (mouse-anti-HA or rabbit-anti GFP) and beads for 2 h at 4°C. Input samples were collected and lysates were then incubated with primary antibodies overnight at 4°C, followed by the addition of 30 μL of washed beads (50% slurry). Sepharose Protein A beads (GE healthcare) were used for the immunoprecipitation of endogenous Beclin-1, Ataxin-3 and VPS34, whereas endogenous ATG14L, UVRAG and Rubicon were immunoprecipitated using magnetic Dynabeads Protein A (Invitrogen). Beads were washed 3X in lysis buffer and proteins were eluted in Laemmli sample buffer by boiling and analyzed by western blot. Endogenous immunoprecipitations were detected with light chain specific antibodies to avoid interference of heavy chain signal, and ratios in endogenous IPs were normalized to input to correct for any differences in input levels. For immunoprecipitation of FLAG-tagged Ataxin-3, cells from 2 wells of a 6-well plate were transfected with 1 μg of 3X-FLAG-Ataxin-3 plasmid (Addgene #22126) each and lysed 1 day post transfection in 100 μL IP buffer with 0,5% NP40. The pooled lysate was diluted and pre-cleared as described above and incubated with 10 μL of magnetic anti-FLAG beads (Sigma) for 2 h at 4°C, followed by washing and elution into sample buffer.

In vitro binding assay with VCP-GST

VCP-GST was purified from *E. coli* and cross-linked to glutathione sepharose beads (Pierce). Empty glutathione beads were used as a control and buffer composition and incubation conditions were optimized to minimize interaction with empty beads and negative control (FLAG-UFD1$_{\Delta VCP}$). 20 μL of VCP-GST cross-linked to beads was incubated with 150-250 ng of FLAG-tagged PI3K proteins in 500 μL binding buffer (25 mM HEPES pH 7.25, 200 mM NaCl, 0.01% Triton X-100, and 5% Glycerol, 1 mM DTT) for 4 h at 4°C. Beads were then washed 4X in binding buffer + 0,1% Tween-20, and bound proteins were eluted in Laemmli sample buffer and analyzed by western blot.

In vitro PI3K assembly

Individual FLAG-tagged proteins (ATG14L and Beclin-1 purified from HEK293; VPS15 and VPS34 purified together from Expi293F suspension cells). 250 ng of each protein was used per reaction, with the exception of VPS34 which was in 5-10X excess compared to VPS15. PI3K proteins were incubated in 500 μL binding buffer in the presence or absence of 500 ng VCP (purified, GST tag removed by PreScission cleavage) for 2 h at 4°C. Assembled PI3K complexes were immunoprecipitated using mouse-anti-ATG14L antibody (MBL). 1,5 μL of primary antibody was added to the reactions, incubated for 1 h at 4°C followed by the addition of 15 μL Protein A Dynabeads. After 2 h, beads were washed 3X in binding buffer and proteins were eluted in sample buffer.

***In vitro* Deubiquitination assay**

Ubiquitinated Beclin-1 was purified from HeLa cells overexpressing 3X-FLAG-Beclin-1 together with HA-Ubiquitin (1:3), treated with proteasome inhibitor MG132 at 10 μM and 10 μM deubiquitinase inhibitor PR619 for 6 h, using FLAG M2 magnetic beads. 1/10 of the amount of Beclin-1-ubq purified from HeLa in a 14 cm^2 plate was mixed with 55 ng of recombinant active VCP-GST (SignalChem) and 12.5 ng of Ataxin-3-GST (BostonBiochem) in 21 μL deubiquitination buffer (Tris pH 8.8 50 mM; NaCl 10 mM; EDTA 1mM; Glycerol 5%) with or without 4 mM of ATP and incubated at 37°C for 5 h. The reaction was stopped by addition of 4 μL 4X Laemmli sample buffer. Ubiquitination was analyzed by western blot using antibody against ubiquitin-HA. Levels of Beclin-1, VCP and Ataxin-3 were analyzed on a separate blot.

Proteomic analysis of Beclin-1 interactors from brain lysate

C57BL/6J mice (Jackson Laboratories) at the age of 6 weeks were sacrificed by a schedule 1 method. The brain was collected and frozen for western blot analysis. Brain tissues were dissected, homogenized and resuspended in tissue lysis buffer on ice (50mM Tris pH 7.4, 0.5% Triton X-100 and protease inhibitor cocktail) and the supernatant was centrifuged twice. Brain lysates were incubated with Beclin-1 antibody (Cell Signaling) or isogenic rabbit IgG control overnight at 4°C followed by 2 h incubation with protein A sepharose beads (GE Healthcare). The immunocomplexes were then washed with lysis buffer three times. Samples were resolved into a Novex pre-cast 4-12% Bis-Tris polyacrylamide gel (Thermo Fisher Scientific). The lanes were excised and cut in 3 approximately equal chunks and the proteins reduced, alkylated and digested in-gel. The resulting tryptic peptides analyzed by LC-MSMS using a Q Exactive coupled to an RSLCnano3000 (Thermo Scientific). Raw files were processed in Proteome Discoverer 1.4 using Sequest to search a mouse Uniprot database. Peptides were filtered to high confidence (0.01 FDR) using Percolator.

In vitro PI(3)P kinase assay

FLAG-tagged PI3K components were co-expressed and purified from HEK293 cells using M2 FLAG agarose beads (Sigma). PI3K complexes on agarose beads were used in in vitro kinase reaction. In vitro kinase reaction and PI(3)P detection was performed using Class III PI3K Elisa Kit (Echelon). 1/10 of PI3K complexes purified from one 14cm^2 dish was used per kinase reaction. Complexes were added to tubes containing kinase buffer (20 mM Tris, 20 mM NaCl, 5mM $MgCl_2$, 10 mM $MnCl_2$, 1 mM EDTA, 50 μM DTT, 0,02% CHAPS) with 0.1 mg/mL sonicated PI substrate, in the presence or absence of 10 ng purified VCP protein (50 μl final reaction volume). Reactions were started by the addition of 50 μM ATP and allowed to continue for 2 h at 37°C before being stopped by the addition of 5 μL of 100 mM EDTA and upon centrifugation, supernatants were transferred to 96-well plates for detection of PI(3)P using instructions for the Class III PI3K Elisa Kit with the following alterations: incubation with PI(3)P detector was reduced to 50 min, and incubation with TMB buffer for developing was extended to 45 min. Upon signal development, plates were read at 450 nM using Spark microplate reader (Tecan).

QUANTIFICATION AND STATISTICAL ANALYSIS

Image Analysis

Puncta analysis (PI(3)P and LC3) was performed in ImageJ, with manual annotation of cell boundaries using ROI and automatic analysis of number of puncta per cell using particle analysis plugin, using the same cut-off for puncta identification in all conditions. A minimum of 60 cells was examined for each condition and experiments were repeated at least three times. For WIPI2 and ATG16L puncta analysis, Cellprofiler software was used. Cell boundaries were determined based on the fluorescence of the proteins analyzed. Automatic analysis of the number and area of the puncta per cell were obtained using IdentifyPrimeryObjects. Same settings were used for the analysis of the puncta in all conditions. Western blots images were quantified by densitometry analysis using ImageStudio Lite software.

Statistical analysis

Significance levels for comparisons between groups were determined with unpaired students t-test or one-way ANOVA for multiple comparisons using GraphPad Prism 8 (GraphPad Software) or Excel (Microsoft office). For western blots, protein levels were normalized to total forms or a housekeeping protein, such as actin or GAPDH. All data is expressed as means ± standard deviation (SD), unless otherwise stated in figure legends. P values of < 0.05 were considered statistically significant. The experiments were appropriately randomized and blinded when possible. More information on statistical analysis is given in figure legends.

Data availability

Authors can confirm that all relevant data are included in the paper and/or its supplementary information files. Further information and requests for resources and reagents should be directed to and will be fulfilled by the Lead Contact, David C. Rubinsztein (dcr1000@cam.ac.uk).

Acknowledgements

We thank Zhenyu Yue for sharing the pFLAG-ATG14L construct, Rolf Schröder and Cristoph Clemen for sharing pGEX-VCP-GST. We thank Per Widlund and Seema Qamar for advice and technical support in protein purification and *in vitro* methods. We thank Farah Siddiqi and Cansu Karabiyik for assistance in brain dissection and primary cultures; Gautam Runwal for cloning the UFD1L$_{\Delta VCP}$ construct, and Robin Antrobus at CIMR proteomics facility for mass spectrometry analysis. We are grateful for funding from the UK Dementia Research Institute (funded by the MRC, Alzheimer's Research UK and the Alzheimer's Society) (UKDRI-2002 to DCR), The

Tau Consortium, Alzheimer's Research UK, an anonymous donation to the Cambridge Centre for Parkinson-Plus, AstraZeneca, the Swedish Natural Research Council (VR) (reference 2016–06605; to S.M.H;) and from the European Molecular Biology Organisation (EMBO long-term fellowships, ALTF 1024-2016 and ALTF 135-2016, to SMH and LW; respectively).

Author contributions

D.C.R conceptualized and supervised the project. Experiments were designed, performed and analyzed by S.M.H, L.W, A.A and M.F-E. R.W.B. and K.T: A.A performed initial experiments on VCP and Beclin-1 interaction, and analyzed effect of *VCP* kd and inhibition on LC3 levels, L.W and M.F-E performed immunofluorescence analysis of early autophagy factors WIPI2, ATG16L and LC3. S.M.H. performed all the in cell and *in vitro* binding studies, PI(3)P detection, *in vitro* deubiquitination, analysis of protein levels, and summarized and compiled all data for the manuscript. R.W.B. and K.T contributed to the design and interpretation of experiments. S.M.H and D.C.R wrote the manuscript with input from L.W. and all the other authors.

Declaration of interests

K.T. and R.W.B were employees of AstraZeneca when the experiments were performed and are shareholders of AstraZeneca. R.W.B is currently employed by Cerevance Ltd. DCR is a consultant for Aladdin Healthcare Technologies Ltd and Nido Biosciences. None of the other authors have competing interests.

References

1 Rubinsztein, D. C., Codogno, P. & Levine, B. Autophagy modulation as a potential therapeutic target for diverse diseases. *Nat Rev Drug Discov* **11**, 709-730, doi:10.1038/nrd3802 (2012).

2 Bento, C. F. *et al.* Mammalian Autophagy: How Does It Work? *Annu Rev Biochem* **85**, 685-713, doi:10.1146/annurev-biochem-060815-014556 (2016).

3 Obara, K., Noda, T., Niimi, K. & Ohsumi, Y. Transport of phosphatidylinositol 3-phosphate into the vacuole via autophagic membranes in Saccharomyces cerevisiae. *Genes Cells* **13**, 537-547, doi:10.1111/j.1365-2443.2008.01188.x (2008).

4 Puri, C., Vicinanza, M. & Rubinsztein, D. C. Phagophores evolve from recycling endosomes. *Autophagy* **14**, 1475-1477, doi:10.1080/15548627.2018.1482148 (2018).

5 Hill, S. M., Wrobel, L. & Rubinsztein, D. C. Post-translational modifications of Beclin 1 provide multiple strategies for autophagy regulation. *Cell Death Differ*, doi:10.1038/s41418-018-0254-9 (2018).

6 Mizushima, N., Sugita, H., Yoshimori, T. & Ohsumi, Y. A new protein conjugation system in human. The counterpart of the yeast Apg12p conjugation system essential for autophagy. *J Biol Chem* **273**, 33889-33892 (1998).

7 Kabeya, Y. *et al.* LC3, a mammalian homologue of yeast Apg8p, is localized in autophagosome membranes after processing. *The EMBO journal* **19**, 5720-5728, doi:10.1093/emboj/19.21.5720 (2000).

8 Klionsky, D. J. *et al.* Guidelines for the use and interpretation of assays for monitoring autophagy (3rd edition). *Autophagy* **12**, 1-222, doi:10.1080/15548627.2015.1100356 (2016).

9 van den Boom, J. & Meyer, H. VCP/p97-Mediated Unfolding as a Principle in Protein Homeostasis and Signaling. *Mol Cell* **69**, 182-194, doi:10.1016/j.molcel.2017.10.028 (2018).

10 Tresse, E. *et al.* VCP/p97 is essential for maturation of ubiquitin-containing autophagosomes and this function is impaired by mutations that cause IBMPFD. *Autophagy* **6**, 217-227 (2010).

11 Ju, J. S., Miller, S. E., Hanson, P. I. & Weihl, C. C. Impaired protein aggregate handling and clearance underlie the pathogenesis of p97/VCP-associated disease. *J Biol Chem* **283**, 30289-30299, doi:10.1074/jbc.M805517200 (2008).

12 Ju, J. S. *et al.* Valosin-containing protein (VCP) is required for autophagy and is disrupted in VCP disease. *The Journal of cell biology* **187**, 875-888, doi:10.1083/jcb.200908115 (2009).

13 Papadopoulos, C. *et al.* VCP/p97 cooperates with YOD1, UBXD1 and PLAA to drive clearance of ruptured lysosomes by autophagy. *The EMBO journal* **36**, 135-150, doi:10.15252/embj.201695148 (2017).

14 Ramanathan, H. N. & Ye, Y. The p97 ATPase associates with EEA1 to regulate the size of early endosomes. *Cell Res* **22**, 346-359, doi:10.1038/cr.2011.80 (2012).

15 Ritz, D. *et al.* Endolysosomal sorting of ubiquitylated caveolin-1 is regulated by VCP and UBXD1 and impaired by VCP disease mutations. *Nature cell biology* **13**, 1116-1123, doi:10.1038/ncb2301 (2011).

16 Chou, T. F. *et al.* Reversible inhibitor of p97, DBeQ, impairs both ubiquitin-dependent and autophagic protein clearance pathways. *Proc Natl Acad Sci U S A* **108**, 4834-4839, doi:10.1073/pnas.1015312108 (2011).

17 Birgisdottir, A. B. & Johansen, T. Autophagy and endocytosis - interconnections and interdependencies. *J Cell Sci* **133**, doi:10.1242/jcs.228114 (2020).

18 Pleasure, I. T., Black, M. M. & Keen, J. H. Valosin-containing protein, VCP, is a ubiquitous clathrin-binding protein. *Nature* **365**, 459-462, doi:10.1038/365459a0 (1993).

19 Ashkenazi, A. *et al.* Polyglutamine tracts regulate beclin 1-dependent autophagy. *Nature* **545**, 108-111, doi:10.1038/nature22078 (2017).

20 Hirabayashi, M. *et al.* VCP/p97 in abnormal protein aggregates, cytoplasmic vacuoles, and cell death, phenotypes relevant to neurodegeneration. *Cell Death Differ* **8**, 977-984, doi:10.1038/sj.cdd.4400907 (2001).
21 Doss-Pepe, E. W., Stenroos, E. S., Johnson, W. G. & Madura, K. Ataxin-3 interactions with rad23 and valosin-containing protein and its associations with ubiquitin chains and the proteasome are consistent with a role in ubiquitin-mediated proteolysis. *Molecular and cellular biology* **23**, 6469-6483 (2003).
22 Wang, Q., Li, L. & Ye, Y. Regulation of retrotranslocation by p97-associated deubiquitinating enzyme ataxin-3. *The Journal of cell biology* **174**, 963-971, doi:10.1083/jcb.200605100 (2006).
23 Laco, M. N., Cortes, L., Travis, S. M., Paulson, H. L. & Rego, A. C. Valosin-containing protein (VCP/p97) is an activator of wild-type ataxin-3. *PLoS One* **7**, e43563, doi:10.1371/journal.pone.0043563 (2012).
24 Sun, Q. *et al.* Identification of Barkor as a mammalian autophagy-specific factor for Beclin 1 and class III phosphatidylinositol 3-kinase. *Proc Natl Acad Sci U S A* **105**, 19211-19216, doi:10.1073/pnas.0810452105 (2008).
25 Song, C., Wang, Q. & Li, C. C. Characterization of the aggregation-prevention activity of p97/valosin-containing protein. *Biochemistry* **46**, 14889-14898, doi:10.1021/bi700499j (2007).
26 Magnaghi, P. *et al.* Covalent and allosteric inhibitors of the ATPase VCP/p97 induce cancer cell death. *Nat Chem Biol* **9**, 548-556, doi:10.1038/nchembio.1313 (2013).
27 Zhou, H. J. *et al.* Discovery of a First-in-Class, Potent, Selective, and Orally Bioavailable Inhibitor of the p97 AAA ATPase (CB-5083). *J Med Chem* **58**, 9480-9497, doi:10.1021/acs.jmedchem.5b01346 (2015).
28 Ravikumar, B., Imarisio, S., Sarkar, S., O'Kane, C. J. & Rubinsztein, D. C. Rab5 modulates aggregation and toxicity of mutant huntingtin through macroautophagy in cell and fly models of Huntington disease. *J Cell Sci* **121**, 1649-1660, doi:10.1242/jcs.025726 (2008).
29 Fu, Q. *et al.* Valosin-containing protein (VCP) promotes the growth, invasion, and metastasis of colorectal cancer through activation of STAT3 signaling. *Mol Cell Biochem* **418**, 189-198, doi:10.1007/s11010-016-2746-6 (2016).
30 Wojcik, C., Yano, M. & DeMartino, G. N. RNA interference of valosin-containing protein (VCP/p97) reveals multiple cellular roles linked to ubiquitin/proteasome-dependent proteolysis. *J Cell Sci* **117**, 281-292, doi:10.1242/jcs.00841 (2004).
31 Dooley, H. C. *et al.* WIPI2 links LC3 conjugation with PI3P, autophagosome formation, and pathogen clearance by recruiting Atg12-5-16L1. *Mol Cell* **55**, 238-252, doi:10.1016/j.molcel.2014.05.021 (2014).
32 Herzog, L. K. *et al.* The Machado-Joseph disease deubiquitylase ataxin-3 interacts with LC3C/GABARAP and promotes autophagy. *Aging Cell* **19**, e13051, doi:10.1111/acel.13051 (2020).
33 Boeddrich, A. *et al.* An arginine/lysine-rich motif is crucial for VCP/p97-mediated modulation of ataxin-3 fibrillogenesis. *The EMBO journal* **25**, 1547-1558, doi:10.1038/sj.emboj.7601043 (2006).
34 Funderburk, S. F., Wang, Q. J. & Yue, Z. The Beclin 1-VPS34 complex--at the crossroads of autophagy and beyond. *Trends Cell Biol* **20**, 355-362, doi:10.1016/j.tcb.2010.03.002 (2010).
35 Itakura, E., Kishi, C., Inoue, K. & Mizushima, N. Beclin 1 forms two distinct phosphatidylinositol 3-kinase complexes with mammalian Atg14 and UVRAG. *Molecular biology of the cell* **19**, 5360-5372, doi:10.1091/mbc.E08-01-0080 (2008).
36 Liang, C. *et al.* Beclin1-binding UVRAG targets the class C Vps complex to coordinate autophagosome maturation and endocytic trafficking. *Nature cell biology* **10**, 776-787, doi:10.1038/ncb1740 (2008).
37 Matsunaga, K. *et al.* Two Beclin 1-binding proteins, Atg14L and Rubicon, reciprocally regulate autophagy at different stages. *Nature cell biology* **11**, 385-396, doi:10.1038/ncb1846 (2009).

38 Zhong, Y. *et al.* Distinct regulation of autophagic activity by Atg14L and Rubicon associated with Beclin 1-phosphatidylinositol-3-kinase complex. *Nature cell biology* **11**, 468-476, doi:10.1038/ncb1854 (2009).

39 Itakura, E. & Mizushima, N. Characterization of autophagosome formation site by a hierarchical analysis of mammalian Atg proteins. *Autophagy* **6**, 764-776 (2010).

40 Bruderer, R. M., Brasseur, C. & Meyer, H. H. The AAA ATPase p97/VCP interacts with its alternative co-factors, Ufd1-Npl4 and p47, through a common bipartite binding mechanism. *J Biol Chem* **279**, 49609-49616, doi:10.1074/jbc.M408695200 (2004).

41 Chou, T. F. *et al.* Specific inhibition of p97/VCP ATPase and kinetic analysis demonstrate interaction between D1 and D2 ATPase domains. *J Mol Biol* **426**, 2886-2899, doi:10.1016/j.jmb.2014.05.022 (2014).

42 Tang, W. K., Odzorig, T., Jin, W. & Xia, D. Structural Basis of p97 Inhibition by the Site-Selective Anticancer Compound CB-5083. *Mol Pharmacol* **95**, 286-293, doi:10.1124/mol.118.114256 (2019).

43 Shiozawa, K. *et al.* The common phospholipid-binding activity of the N-terminal domains of PEX1 and VCP/p97. *FEBS J* **273**, 4959-4971, doi:10.1111/j.1742-4658.2006.05494.x (2006).

44 Pecheur, E. I. *et al.* Phospholipid species act as modulators in p97/p47-mediated fusion of Golgi membranes. *Biochemistry* **41**, 9813-9823 (2002).

45 Nascimbeni, A. C., Codogno, P. & Morel, E. Phosphatidylinositol-3-phosphate in the regulation of autophagy membrane dynamics. *FEBS J* **284**, 1267-1278, doi:10.1111/febs.13987 (2017).

46 Chan, N. *et al.* Valosin-containing protein mutation and Parkinson's disease. *Parkinsonism Relat Disord* **18**, 107-109, doi:10.1016/j.parkreldis.2011.07.006 (2012).

47 Johnson, J. O. *et al.* Exome sequencing reveals VCP mutations as a cause of familial ALS. *Neuron* **68**, 857-864, doi:10.1016/j.neuron.2010.11.036 (2010).

48 Darwich, N. F. *et al.* Autosomal dominant VCP hypomorph mutation impairs disaggregation of PHF-tau. *Science*, eaay8826, doi:10.1126/science.aay8826 (2020).

49 Ghosh, D. K., Roy, A. & Ranjan, A. The ATPase VCP/p97 functions as a disaggregase against toxic Huntingtin-exon1 aggregates. *FEBS Letters* **592**, 2680-2692, doi:10.1002/1873-3468.13213 (2018).

50 Wang, B. *et al.* ULK1 and ULK2 Regulate Stress Granule Disassembly Through Phosphorylation and Activation of VCP/p97. *Mol Cell* **74**, 742-757 e748, doi:10.1016/j.molcel.2019.03.027 (2019).

51 Arhzaouy, K. *et al.* VCP maintains lysosomal homeostasis and TFEB activity in differentiated skeletal muscle. *Autophagy* **15**, 1082-1099, doi:10.1080/15548627.2019.1569933 (2019).

52 Chan, N. C. *et al.* Degradation of the deubiquitinating enzyme USP33 is mediated by p97 and the ubiquitin ligase HERC2. *J Biol Chem* **289**, 19789-19798, doi:10.1074/jbc.M114.569392 (2014).

53 Steffen, J. *et al.* Rapid degradation of mutant SLC25A46 by the ubiquitin-proteasome system results in MFN1/2-mediated hyperfusion of mitochondria. *Molecular biology of the cell* **28**, 600-612, doi:10.1091/mbc.E16-07-0545 (2017).

54 McLelland, G. L. *et al.* Mfn2 ubiquitination by PINK1/parkin gates the p97-dependent release of ER from mitochondria to drive mitophagy. *Elife* **7**, doi:10.7554/eLife.32866 (2018).

55 Singh, A. N. *et al.* The p97-Ataxin 3 complex regulates homeostasis of the DNA damage response E3 ubiquitin ligase RNF8. *The EMBO journal* **38**, e102361, doi:10.15252/embj.2019102361 (2019).

56 Ganji, R., Mukkavalli, S., Somanji, F. & Raman, M. The VCP-UBXN1 Complex Mediates Triage of Ubiquitylated Cytosolic Proteins Bound to the BAG6 Complex. *Molecular and cellular biology* **38**, doi:10.1128/MCB.00154-18 (2018).

57 Nguyen, T. V. *et al*. p97/VCP promotes degradation of CRBN substrate glutamine synthetase and neosubstrates. *Proc Natl Acad Sci U S A* **114**, 3565-3571, doi:10.1073/pnas.1700949114 (2017).
58 Hammond, G. R., Schiavo, G. & Irvine, R. F. Immunocytochemical techniques reveal multiple, distinct cellular pools of PtdIns4P and PtdIns(4,5)P(2). *Biochem J* **422**, 23-35, doi:10.1042/BJ20090428 (2009).

References online methods

51 Arhzaouy, K. *et al.* VCP maintains lysosomal homeostasis and TFEB activity in differentiated skeletal muscle. *Autophagy* **15**, 1082-1099, doi:10.1080/15548627.2019.1569933 (2019).

52 Chan, N. C. *et al.* Degradation of the deubiquitinating enzyme USP33 is mediated by p97 and the ubiquitin ligase HERC2. *J Biol Chem* **289**, 19789-19798, doi:10.1074/jbc.M114.569392 (2014).

53 Steffen, J. *et al.* Rapid degradation of mutant SLC25A46 by the ubiquitin-proteasome system results in MFN1/2-mediated hyperfusion of mitochondria. *Molecular biology of the cell* **28**, 600-612, doi:10.1091/mbc.E16-07-0545 (2017).

54 McLelland, G. L. *et al.* Mfn2 ubiquitination by PINK1/parkin gates the p97-dependent release of ER from mitochondria to drive mitophagy. *Elife* **7**, doi:10.7554/eLife.32866 (2018).

55 Singh, A. N. *et al.* The p97-Ataxin 3 complex regulates homeostasis of the DNA damage response E3 ubiquitin ligase RNF8. *The EMBO journal* **38**, e102361, doi:10.15252/embj.2019102361 (2019).

56 Ganji, R., Mukkavalli, S., Somanji, F. & Raman, M. The VCP-UBXN1 Complex Mediates Triage of Ubiquitylated Cytosolic Proteins Bound to the BAG6 Complex. *Molecular and cellular biology* **38**, doi:10.1128/MCB.00154-18 (2018).

57 Nguyen, T. V. *et al.* p97/VCP promotes degradation of CRBN substrate glutamine synthetase and neosubstrates. *Proc Natl Acad Sci U S A* **114**, 3565-3571, doi:10.1073/pnas.1700949114 (2017).

58 Hammond, G. R., Schiavo, G. & Irvine, R. F. Immunocytochemical techniques reveal multiple, distinct cellular pools of PtdIns4P and PtdIns(4,5)P(2). *Biochem J* **422**, 23-35, doi:10.1042/BJ20090428 (2009).

Figure legends

Figure 1. VCP interacts with Beclin-1 and regulates autophagy initiation

(a) Immunoprecipitation of endogenous Beclin-1 from HeLa cells (two replicates, a and b). (b, c) DBeQ increases LC3-II levels in DMSO conditions, but decreases upon treatment with Bafilomycin A1 (BafA; 400 nM) in basal conditions (b; n=3, -BafA p=0.0009, +BafA p= 0.0328) and in HBSS starvation conditions (c; n=3, -BafA p= 0.0005, +BafA P= 0.0005). Cells were treated with BafA for 1 h prior to addition of 10 μM DBeQ (5 h) in basal media or starvation (HBSS). Graphs represent LC3-II/actin ratios, normalized to DMSO control. (d, e) DBeQ impairs starvation-induced autophagy. HeLa cells were pretreated with BafA (2 h), before transition to starvation media (HBSS) with BafA, combined with addition of DMSO or 10 μM DBeQ (3 h); n=4, number of cells counted: 30-65 per condition, DMSO vs HBSS p= 0.0201, HBSS vs HBSS+DBeQ p=0.0474. Representative images of immunofluorescence analysis of LC3 puncta formation during starvation shown in (e). (f) VCP inhibition impairs formation of PI(3)P puncta upon starvation. HeLa cells were pretreated with 10 μM DBeQ or with wortmannin (Wm; 1μM) prior to starvation (HBSS 1 h); n=3, number of cells counted: 40-60 per condition, DMEM vs HBSS p= 0.0025, HBSS vs HBSS+DBeQ p= 0.0026, HBSS vs HBSS+Wm p= 0.0036. Representative microscopy frames shown in Extended data Fig. 2d. (b-d; f) Data in bar graphs presented as normalized mean ± SD, *p<0.05, **p < 0.005, ***p < 0.0005, unpaired two-tailed Students t-test. Scale bar = 10 μm. See also Extended data Figures 1-3.

Figure 2. VCP governs the recruitment of early autophagy markers

(a, b) DBeQ reduced accumulation of early autophagy marker WIPI2 during starvation. HeLa cells in basal media (DMEM) compared to cells subjected to starvation (HBSS 2 h) in combination with DMSO or DBeQ (10 μM). Median area of WIPI2 signal per cell quantified and normalized to control; n=3, number of cells counted: 30-40 per condition, DMEM vs HBSS p= 0.0072, HBSS vs HBSS+DBeQ p= 0.0076. Representative microscopy frames shown in (b). (c, d) Inhibition of starvation induced ATG16 puncta by VCP inhibition. HBSS 2 h, in combination with DMSO or DBeQ (10 μM). Median area of ATG16 per cell quantified and normalized to control, n=4, number of cells counted: 30-40 per condition, DMEM vs HBSS p= 0.0041, HBSS vs HBSS+DBeQ p= 0.02656. Representative microscopy frames shown in (d). (a, c) Bar graphs data presented as normalized mean ± SD. *p<0.05, **p < 0.005,

unpaired two-tailed Students t-test. Scale bar = 10 μm. See also Extended data Figure 4.

Figure 3. VCP regulates Beclin-1 levels by stabilization and activation of Ataxin-3

(a) Beclin-1 levels in primary mouse neurons after DBeQ (10 μM) treatment for 5 h; n=3, $p< 0.0001$.(b) Beclin-1 levels in HeLa cells after treatment with VCP inhibitor DBeQ (10 μM for 8 h). Cells were co-treated with cycloheximide (CHX, 50 μg/ml) +/- proteasome inhibitor MG132, n=4, $p= 0.0002$. (c) Immunoprecipitation of endogenous Ataxin-3 from HeLa cells, treated with DBeQ (10 μM, 5 h), ratio of Beclin-1 to Ataxin-3 normalized to input levels displayed below graph. Experiment was repeated twice. (d, e) Beclin-1 levels upon overexpression of Ataxin-$3_{\Delta VCP}$ or wildtype Ataxin-3. Beclin-1-FLAG was overexpressed together with empty vector, Ataxin-3-FLAG or Ataxin-$3_{\Delta VCP}$-FLAG in the presence of CHX and MG132. Quantification of Beclin-1 to Actin levels presented in (e); n=4, -MG132: FLAG vs Ataxin-3 $p= 0.00011$, Ataxin-3 vs Ataxin-$3_{\Delta VCP}$ $p= 0.0014$. (f) HeLa cells are treated with control siRNA or siRNA for *ATAXIN-3*, followed by reconstitution with Ataxin-3 or Ataxin-$3_{\Delta VCP}$ and subjected to immunofluorescence microscopy. Number of LC3 puncta per cell quantified and normalized to wildtype Ataxin-3; n=3, $p= 0.0114$. See also Extended data Fig. 6a-b for microscopy images and scatter plot from a representative experiment. (g) *In vitro* deubiquitination of Beclin-1 upon addition of purified Ataxin-3 with and without addition of purified VCP in the presence or absence of ATP. Levels of ubiquitinated Beclin-1 were quantified; n=3, +ATP samples: control vs Ataxin-3 $p= 0.01186$, control vs Ataxin-3+VCP $p= 0.000375$, control vs VCP $p= 0.000218$, Ataxin-3 vs Ataxin-3+VCP $p=0.02173$, Ataxin-3+VCP vs VCP $p=0.02836$. Representative gel image in Extended data Fig. 6c. (a, b, e-g) Bar graphs data presented as normalized mean ± SD. *p<0.05, **$p < 0.005$, ***$p < 0.0005$, unpaired two-tailed Students t-test. See also Extended data Figure 5 and 6.

Figure 4. Interaction of VCP with PI(3)P-producing Beclin-1 complexes

(a) Endogenous UVRAG, ATG14L and Rubicon were immunoprecipitated from HeLa cells. (b) Immunoprecipitation of endogenous ATG14L in cells treated with control siRNA or siRNA against *ATAXIN-3*. (c) Immunoprecipitation of ATG14L in control cells versus cells treated with siRNA against *BECLIN-1*. (d) Immunoprecipitation of Ataxin-3-FLAG in cells treated with control siRNA, or siRNA against *BECLIN-1*. Cells

in (c-d) overexpress *ATG14L* (c,d) and *ATAXIN-3-FLAG* (d), and IP ratios have been normalized to input ratios to account for difference in input protein levels. (e) *In vitro* PI(3)P production by PI3K complexes in the presence of absence of purified VCP. The VPS34 inhibitor IN1 (1μM) was used as a control. Bar graph data presented as normalized mean ± SD, n=3-4, *$p < 0.05$, **$p < 0.005$, ***$p < 0.0005$, one-way ANOVA with Fisher's LSD test, PI3K vs VCP $p<0.001$, PI3K vs PI3K+VCP $p=0.005$, PI3K vs PI3K+IN1 $p=0.012$. See also Extended Data Fig. 7.

Figure 5. VCP regulates the assembly of PI3K complexes

(a) Immunoprecipitation of endogenous ATG14L from HeLa cells treated with DMSO, 10 μM NMS873, 5 μM CB-5083 or 10 μM DBeQ for 6 h. (b) Amount of proteins co-immunoprecipitated with ATG14L in the denoted conditions, ratioed to the amount in input sample and normalized to DMSO control; n=4, for NMS873 sample: VCP p = 0.04275, VPS34 p = 0.00410, Beclin-1 p = 0.00263; for CB-5083: Beclin-1 p= 0.04861; for DBeQ: VCP p = 0.019, VPS15 p = 0.00172, VPS34 p = 0.04765, Beclin-1 p = 0.006. (c) *In vitro* assembly of PI3K complexes. FLAG-tagged PI3K components were added individually (VPS15 and VPS34 purified and added together) and incubated alone or together with purified VCP, followed by immunoprecipitation of ATG14L. (d) Ratios of proteins co-immunoprecipitated with ATG14L in the denoted conditions *in vitro*, normalized to ratios in DMSO control; n=7, VPS15 p = 0.006, VPS34 p = 0.004, Beclin-1 p = 0.025. (e) Schematic illustrating the dual role of VCP in autophagy initiation. VCP binds Ataxin-3 and Beclin-1 and stimulates deubiquitination of Beclin-1, and thereby stabilizes Beclin-1 protein levels. VCP also binds to other components of the PI3K complex and enhances its assembly and activity. Inhibition of VCP with CB-5083, NMS873 or DBeQ perturbs both functions. (b, d) Bar graphs data presented as normalized mean ± SD. *$p < 0.05$, **$p < 0.005$, unpaired two-tailed Students t-test. See also Extended Data Fig. 8.

EXTENDED DATA

Extended Data Figure 1. VCP interacts with Beclin-1 *in vivo* and *in vitro*.

(a) Schematic overview of Beclin-1 protein domains; with the N-terminal domain in dark grey, coiled-coiled domain (CCD) in blue, and the beta-alpha repeated, autophagy-specific (BARA) domain in light grey. Depicted below is the different truncation mutants used for binding studies (all with N-terminal FLAG tag). (b) *In vitro* binding of FLAG-tagged Beclin-1 truncation mutants to VCP-GST crosslinked to beads. Empty Glutathione beads and mutated VCP interactor UFD1L (Δaa215-241; $UFD1L_{\Delta VCP}$), were used as a negative control in binding experiments. Ratio of bound protein bound to VCP-GST was quantified by detection of FLAG signal in bound fraction divided by input signal and normalized to the full-length control; n=5, $UFD1L_{\Delta VCP}$ p= 0.0031. (c) Representative gel of *in vitro* binding experiment quantified in (b). (d) DBeQ impairs autophagic flux and autophagosome formation during starvation (HBSS, 4 h) in primary neurons, as demonstrated by LC3-II levels in conditions without and with 1 h pre-treatment with Bafilomycin A1 (BafA; 400 nM); n=3, -BafA p = 0.00105, +BafA p = 0.00005. (b, d) Bar graphs data presented as normalized mean ± SD, **p < 0.005, ***p < 0.0005, unpaired two-tailed Students t-test. See also main Figure 1.

Extended Data Figure 2. VCP regulates early autophagy initiation.

(a) LC3 puncta formation upon treatment with VCP inhibitors. HeLa cells were pretreated with BafA (2 h), before transition to HBSS (+ BafA), with addition of DMSO, 10 μM NMS873 or 5 μM CB-5083 for 3 h. Number of LC3 puncta per cell normalized to DMEM control; n=3, number of cells counted: 50-60 per condition, one-way ANOVA with Dunnett's correction for multiple comparisons, DMEM vs HBSS+DMSO p = 0.049, HBSS+DMSO vs HBSS+NMS873 p = 0.009, HBSS+DMSO vs HBSS+CB-5083 p = 0.012. (b) Size of LC3 puncta during starvation and VCP inhibition; n=3. (c) Representative images of LC3 puncta formation, as quantified in (a) and (b). (d) Representative images for PI(3)P puncta formation upon starvation (HBSS 1 h) in HeLa cells, with and without treatment with the VPS34 inhibitor Wm (1μM) as quantified in main Fig.1f. (e) Representative images for PI(3)P puncta formation upon starvation (HBSS 1 h) in HeLa cells, with and without treatment with 10 μM NMS873 or 5 μM CB-5083 compared to DMSO in basal media (DMEM) as quantified in (f, g). (f) Quantification of number of PI(3)P puncta per cell during starvation and VCP inhibition normalized to DMEM control; n=4, number of cells

counted: 40-50 per condition, one-way ANOVA with Dunnett's correction for multiple comparisons: DMEM vs HBSS p= 0.003, HBSS vs HBSS+NMS873 p < 0,001, HBSS vs HBSS+2 μM CB-5083 p= 0.016, HBSS vs HBSS+5 μM CB-5083 p < 0,001, HBSS vs HBSS+IN1 p= 0.002. (g) Quantification of size of PI(3)P puncta per cell from experiment in (f); one-way ANOVA with Dunnett's correction for multiple comparisons: HBSS vs HBSS+NMS873 p= 0.033, HBSS vs HBSS+2 μM CB-5083 p= 0.049, HBSS vs HBSS+5 μM CB-5083 p=0.049, HBSS vs HBSS+IN1 p= 0.026. (h) ATG5-ATG12 conjugation in HeLa cells treated with siRNA to knockdown expression of *VCP*; n=3, unpaired two-tailed Student t-test, VCP siRNA 11 p= 0.0009, VCP siRNA 12 P= 0.0007. (a, b, f-h) Data in bar graphs presented as normalized mean ± SD. *p<0.05, **p<0.005, ***p < 0.0005. Scale bar = 10 μm. See also main Figure 1.

Extended Data Figure 3. Knockdown of *VCP* affects autophagy initiation

(a) Knockdown of *VCP* impairs PI(3)P production upon starvation. HeLa cells treated with control siRNA (ctrl) or siRNA targeting *VCP* were starved (HBSS 1 h) 48 h post transfection and stained for nuclei (DAPI, blue), VCP levels (green) and PI(3)P production (red). (b) Quantified data for experiment in (a), shown as normalized mean ± SD, n= 3, number of cells counted: 40-50 per condition, unpaired two-tailed Students t-test, DMEM vs HBSS p= 0.03855, HBSS vs kd VCP p= 0.04527. (c) LC3-II levels upon *VCP* knockdown in the absence and presence of BafA (400 nM). Efficiency of *VCP* kd tested in separate blot, before cells were divided into -BafA and +BafA conditions. (d) Quantified data for LC3-II levels for experiment in (c), shown as normalized mean ± SD, n= 4, -BafA VCP siRNA 11 p= 0.00058, -BafA VCP siRNA 12 p= 0.00046. *p<0.05, **p < 0.005, ***p < 0.0005. Scale bar = 10 uM. See also main Figure 1.

Extended Data Figure 4. VCP regulates the recruitment of early autophagy markers during starvation and mTOR inhibition.

(a) Immunofluorescent analysis of WIPI2 puncta formation upon starvation with VCP inhibition. HeLa cells in basal media (DMEM) compared to cells subjected to starvation (HBSS 2 h) in combination with DMSO, 10 μM NMS873 or 5 μM CB-5083. Median area of WIPI2 signal per cell normalized to control; n=5, number of cells counted: 30-40 per condition, DMEM+DMSO vs HBSS+DMSO p=0.0076, HBSS+DMSO vs HBSS+NMS873 p=0.0223, HBSS+DMSO vs HBSS+CB-5083 p=0.0253. (b) Immunofluorescent analysis of ATG16 puncta formation upon

starvation during VCP inhibition. HBSS 2 h, in combination with DMSO, 10 μM NMS873 or 5 μM CB-5083. Median area of ATG16 per cell normalized to control; n=4, number of cells counted: 30-40 per condition, DMEM+DMSO vs HBSS+DMSO p=0.0036, HBSS+DMSO vs HBSS+NMS873 p= 0.0033, HBSS+DMSO vs HBSS+CB-5083 p=0.0006. (c) Immunofluorescent analysis of LC3 puncta induction upon mTOR inhibition by Torin 1. HeLa cells pre-treated with BafA (400 nM) together with DMSO, 10 μM NMS873 or 5 μM CB-5083 for 1 h, were subjected to Torin 1 (1 μM) treatment for 4 h. Median area of LC3 per cell normalized to control; n=3, number of cells counted: 30-40 per condition, DMSO vs Torin 1 p= 0.0021, Torin 1 vs Torin 1+NMS873 p= 0.0035, Torin 1 vs Torin 1+CB-5083 p= 0.0034. (a-c) Bar graphs data presented as normalized mean ± SD, *p<0.05, **p < 0.005, unpaired two-tailed students t-test. (d) Representative images of WIPI2 puncta formation upon starvation, as quantified in (a). (e) Representative images of ATG16 puncta formation, as quantified in (b). (f) LC3 puncta formation upon Torin 1 treatment, as quantified in (c). Scale bar = 10 μm. See also main Figure 2.

Extended Data Figure 5. VCP regulates levels of Beclin-1 via Ataxin-3.

(a) Beclin-1 levels in HeLa cells after knockdown of *VCP* compared to control cells transfected with non-targeting siRNA; n=3, VCP siRNA 11 p= 0.00158, VCP siRNA 12 p<0.0001. (b) Beclin-1 levels in HeLa cells upon treatment with DMSO, 10 μM NMS873 or 5 μM CB-5083 for 5 h; n=7, NMS873 p= 0.00013, CB-5083 p= 0.00319. (c) Ataxin-3 levels in HeLa cells upon treatment with DMSO, 10 μM NMS873 or 5 μM CB-5083 for 5 h; n=3, NMS873 p= 0.0002, CB-5083 p= 0.0055. (a-c) Bar graphs represent Beclin-1 or Ataxin-3 to loading control (Actin or GAPDH) ratios displayed as mean ± SD normalized to control, *p<0.05, **p < 0.005, ***p < 0.0005, unpaired two-tailed students t-test. (d) FLAG-tagged Ataxin-3 or mutated version Ataxin-3 $_{\Delta VCP}$ were expressed together with VCP-HA, followed by FLAG immunoprecipitation. (e) Immunoprecipitation of FLAG proteins from cells expressing empty FLAG, FLAG-tagged Ataxin-3 or Ataxin-3 $_{\Delta VCP}$. See also main Figure 3.

Extended Data Figure 6. VCP regulates Ataxin-3 deubiquitinase activity towards Beclin-1.

(a, b) Representative experiment from main Fig. 3f: LC3 puncta per cell in HeLa cells depleted of Ataxin-3 and reconstituted with wildtype Ataxin-3 or Ataxin-3$_{\Delta VCP}$, n=60-

80 cells analyzed per condition. Scale bar = 10 μm. (c) Representative gel image of *in vitro* deubiquitination assay, quantified in main Fig. 3g. See also main Figure 3.

Extended Data Figure 7. VCP interacts with PI3K complexes *in vitro.*

(a) Immunoprecipitation of Ataxin-3-FLAG in control and *VCP* knockdown cells, overexpressing FLAG-Ataxin-3 and ATG14L. IP ratios are normalized to input to account for differences in input protein levels. (b) Protein-stained gel with individually purified FLAG-tagged PI3K components. (c) Protein-stained gel of VCP-GST purified from *E. coli* and cross-linked to glutathione agarose beads. (d) *In vitro* immunoprecipitation with VCP-GST beads and individually purified PI3K components: VPS34, ATG14L, Beclin-1 and $UFD1L_{\Delta VCP}$ (Δaa215-241) as a negative control. Experiment was repeated 6 times.

Extended Data Figure 8. VCP interacts with PI3K complex I.

(a) FLAG-tagged PI3K complexes purified from HEK293 cells. Protein-stained gel (left) and FLAG-probed western blot (right). (b) Quantification of immunoprecipitation of endogenous ATG14L in control cells and in *VCP* knockdown cells. IP ratios have been normalized to input ratios. Representative gel in (c); n=3, unpaired two-tailed student t-test, bar graph data presented as normalized mean ± SD, kd VCP Beclin-1 p=0.0127, kd VCP VPS34 p=0.0041.(d) VCP levels in input samples from endogenous immunoprecipitation of ATG14L with short and long exposure (SE and LE). VCP upper band denoted by red arrow. (e) Short and long exposures of VCP levels from *VCP* kd experiments. Quantifications shown below blots, normalized to levels in control sample. (f) Purification of FLAG-VPS15 and FLAG-VPS34 from 293Expi cells. Purified proteins are visualized with protein stain (instant blue; left lane) and by western blot analysis using FLAG antibody (middle lane). The same membrane was cut and probed with individual antibodies for VPS15, VPS34, ATG14L and Beclin-1 (right lane). See also main Figures 4 and 5.

Figure 1. VCP interacts with Beclin-1 and regulates autophagy initiation

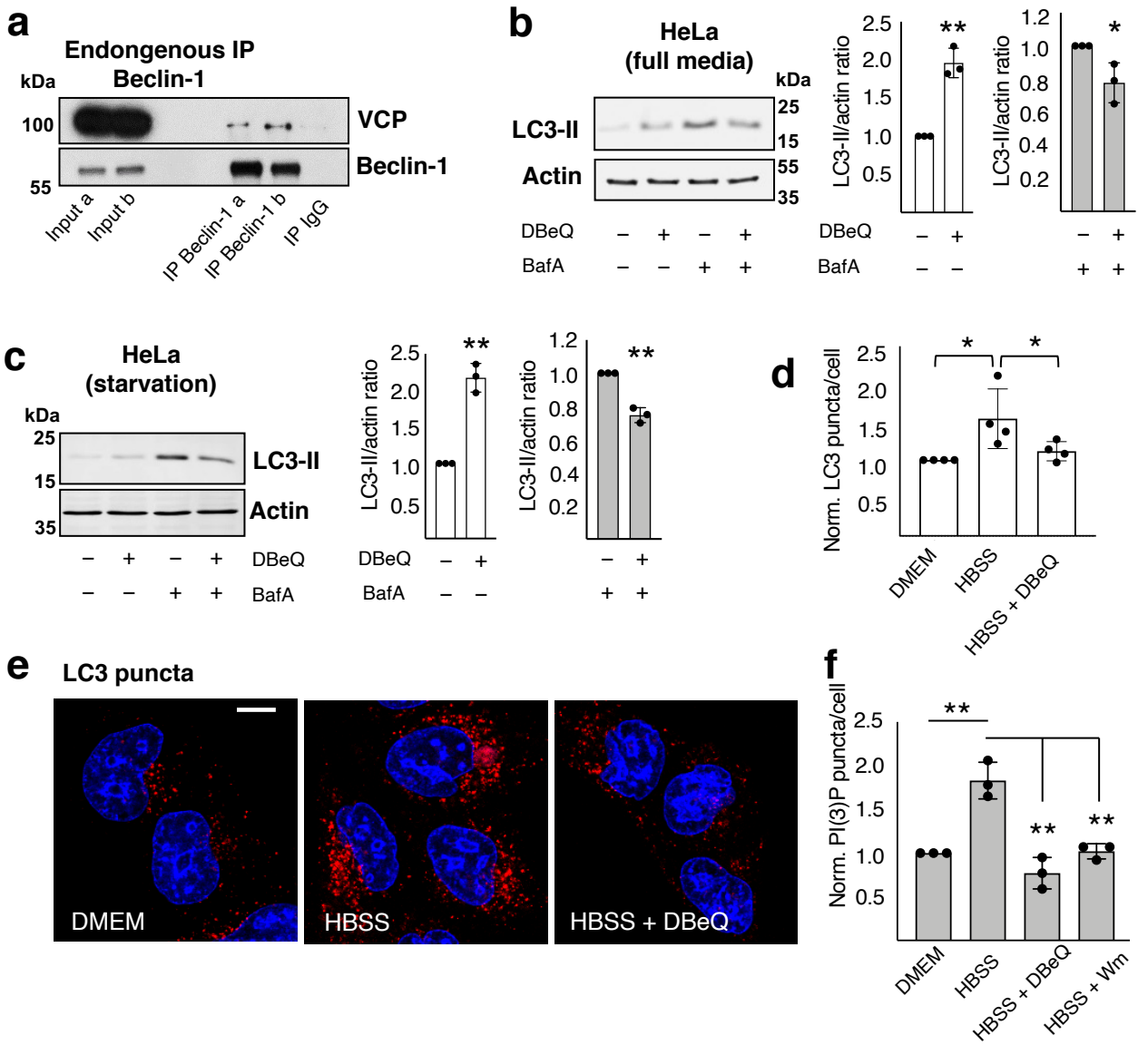

Figure 2. VCP governs the recruitment of early autophagy markers

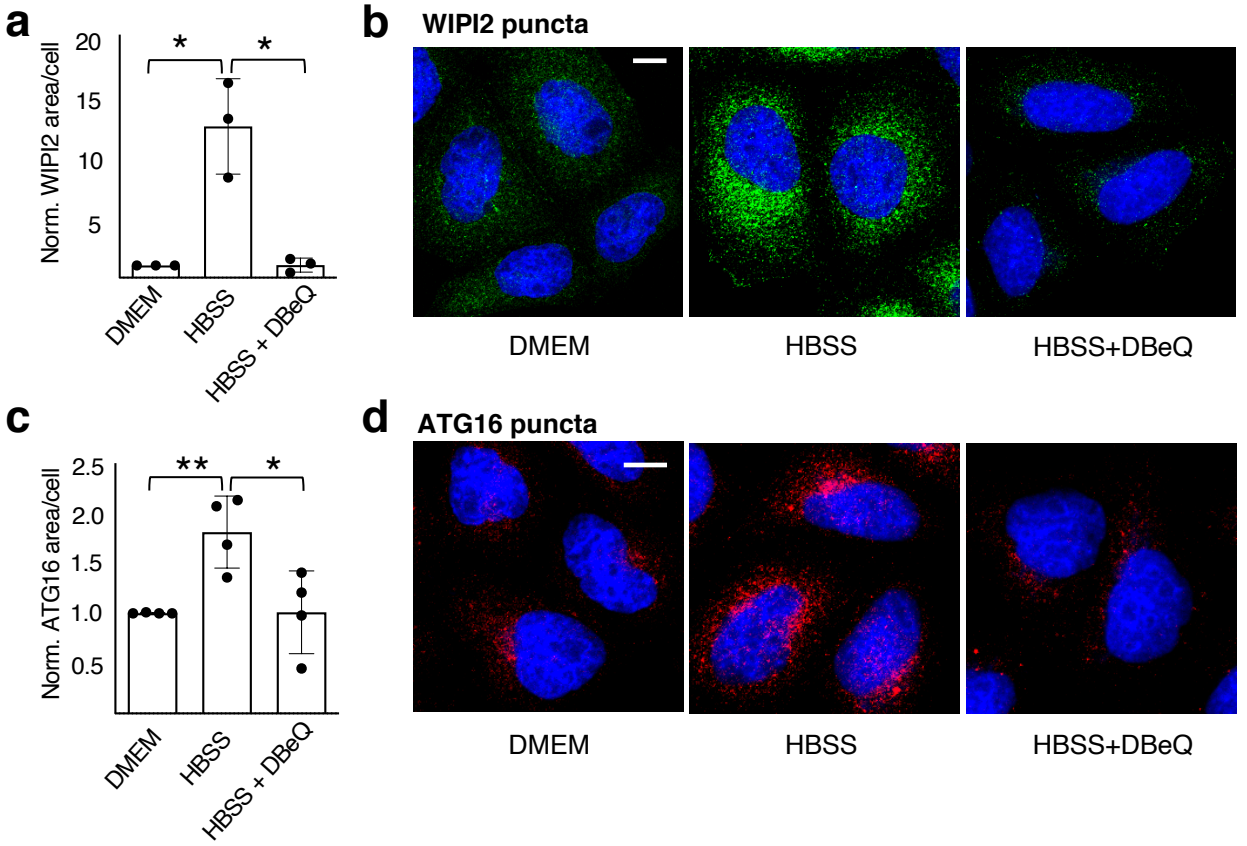

Figure 3. VCP regulates Beclin-1 levels by stabilization and activation of Ataxin-3

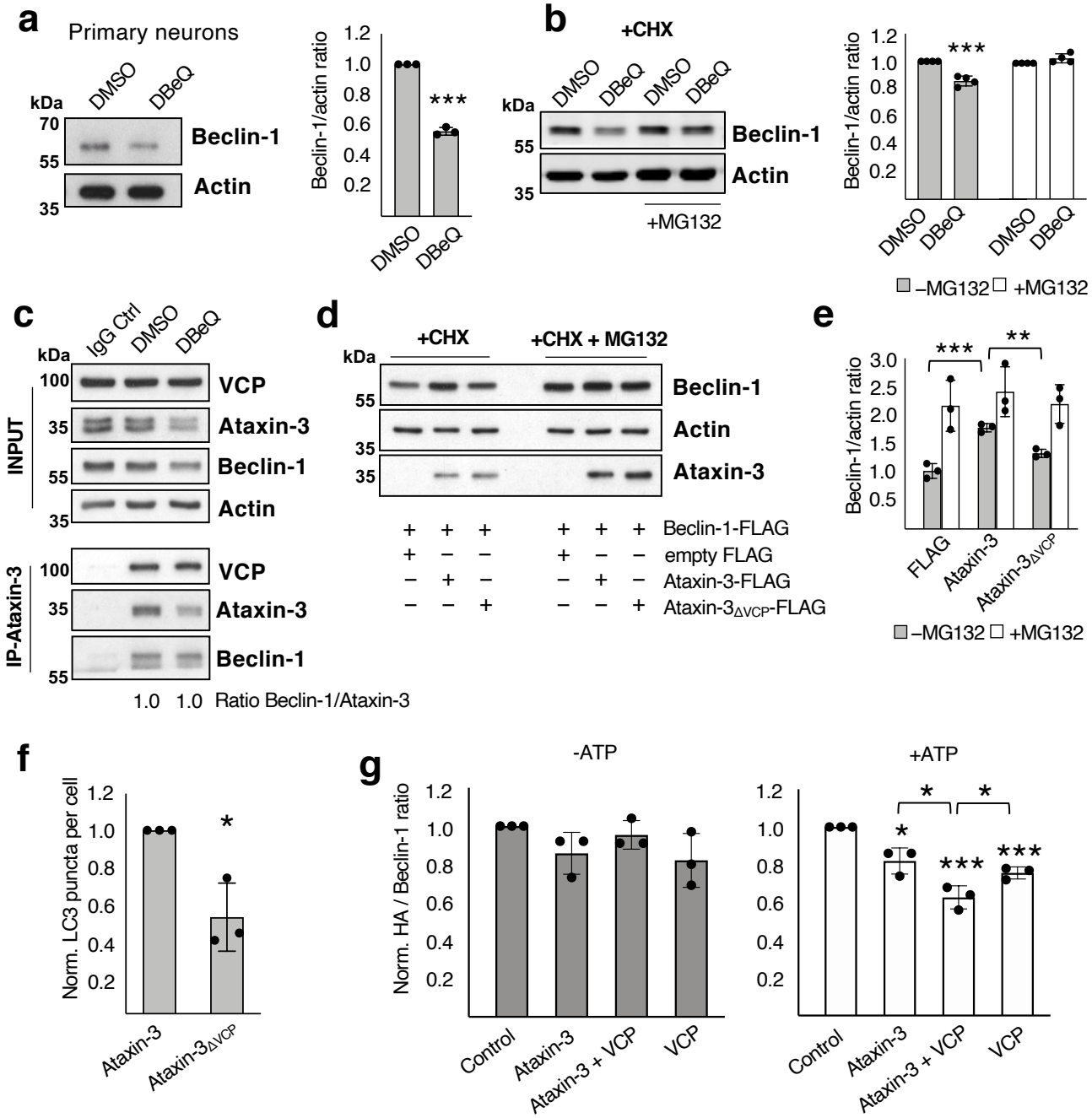

Figure 4. Interaction of VCP with PI(3)P-producing Beclin-1 complexes

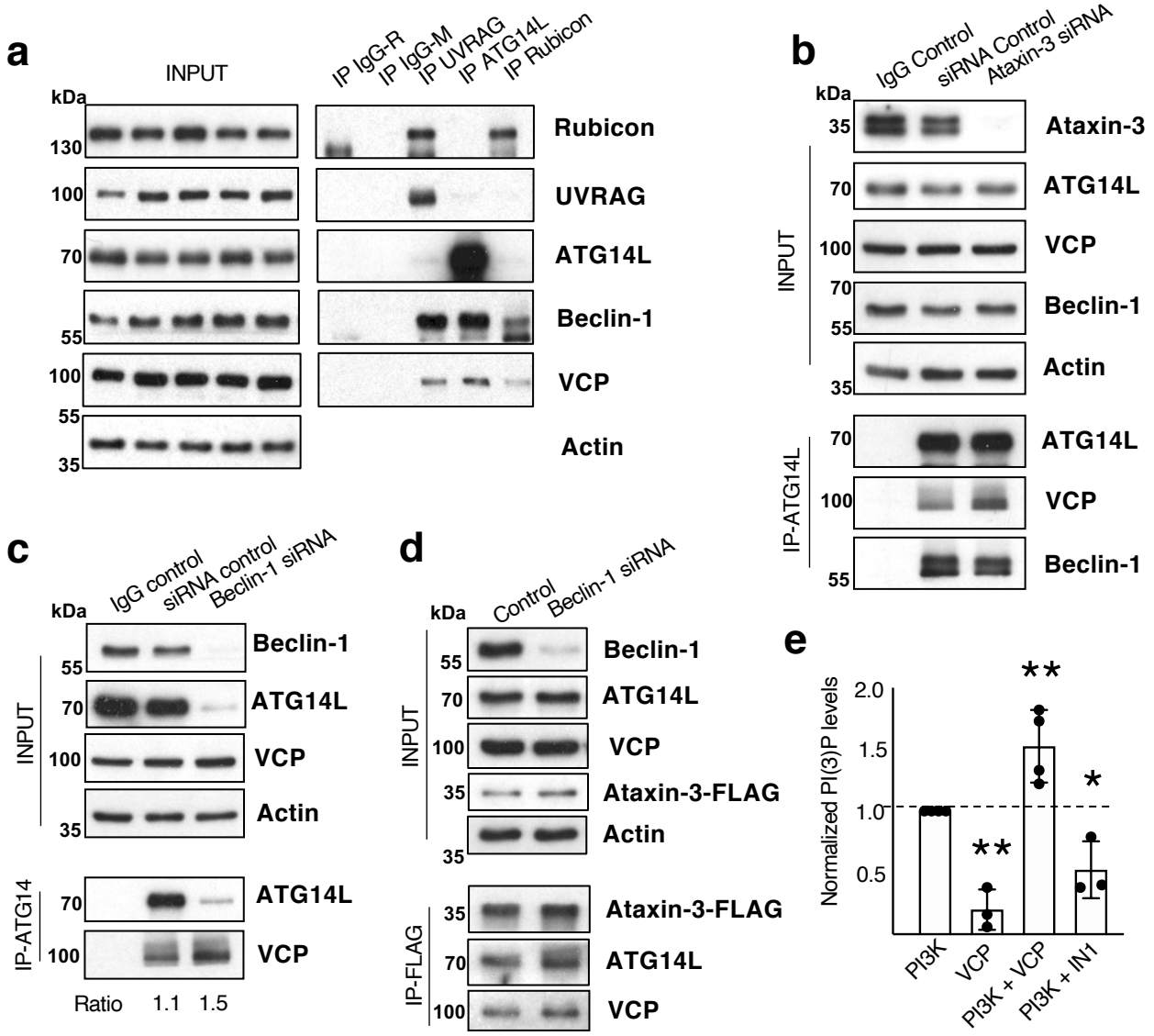

Figure 5. VCP regulates the assembly of PI3K complexes

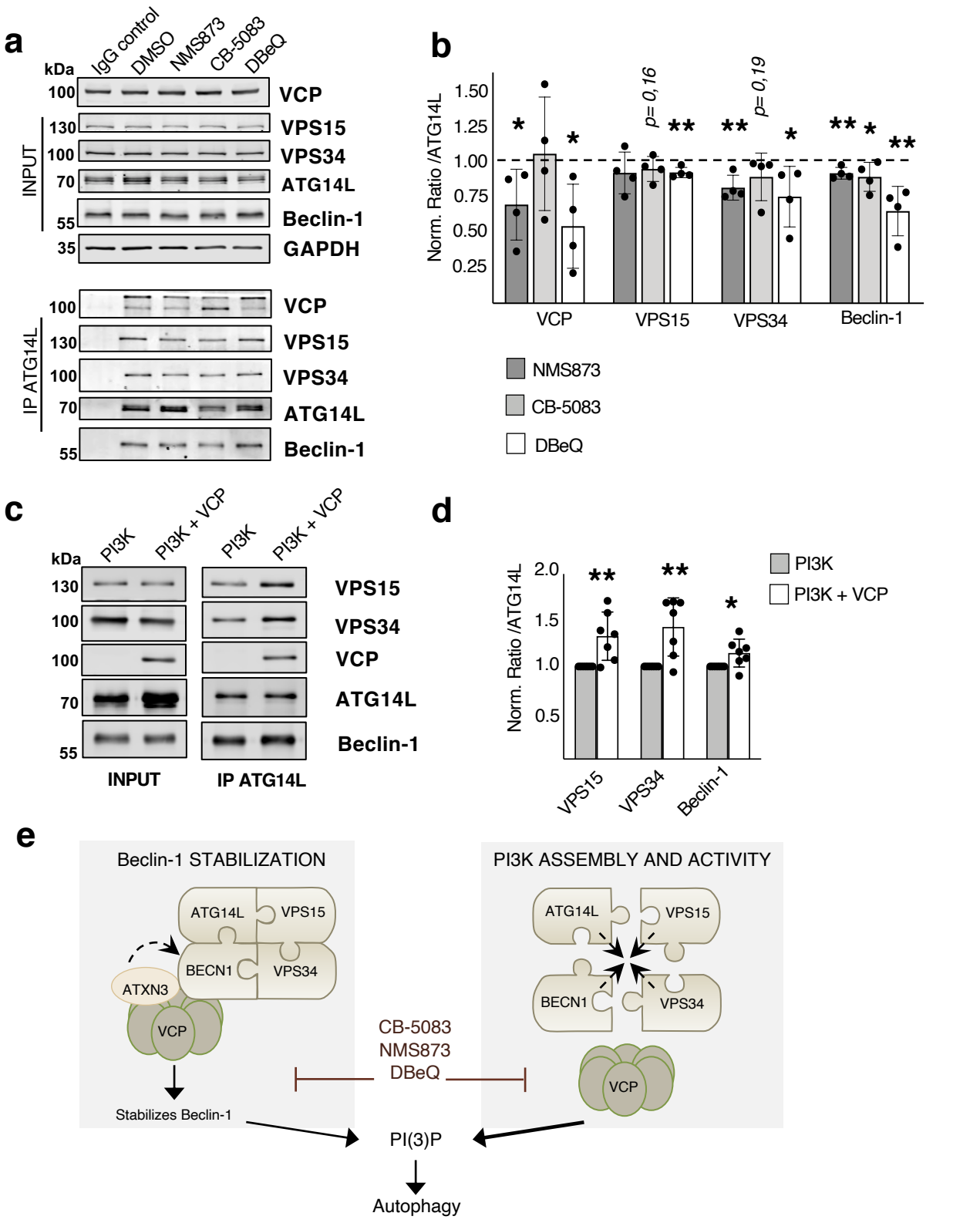

Extended Data Figure 1. VCP interacts with Beclin-1 *in vivo* and *in vitro*

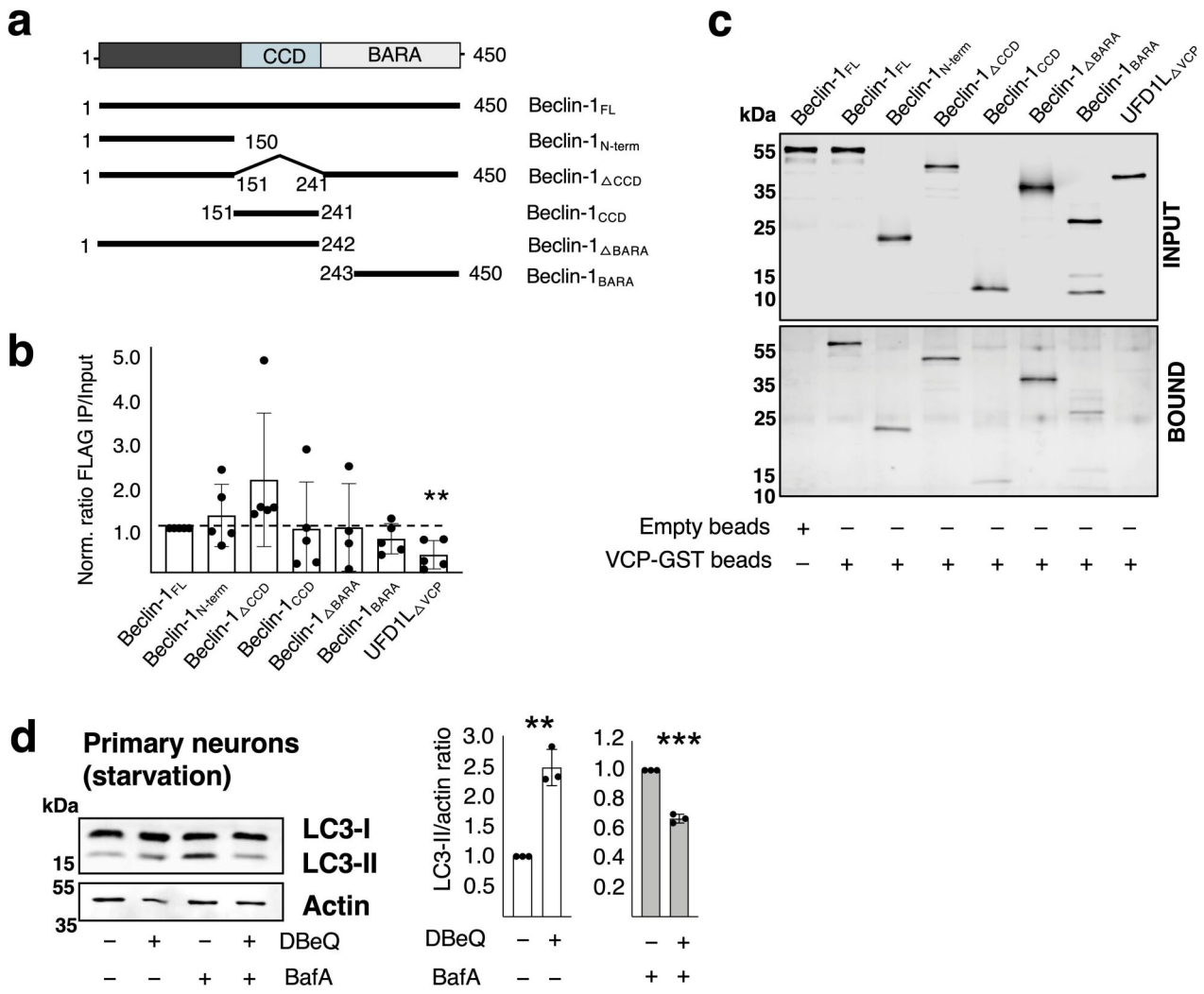

Extended Data Figure 2. VCP regulates early autophagy initiation

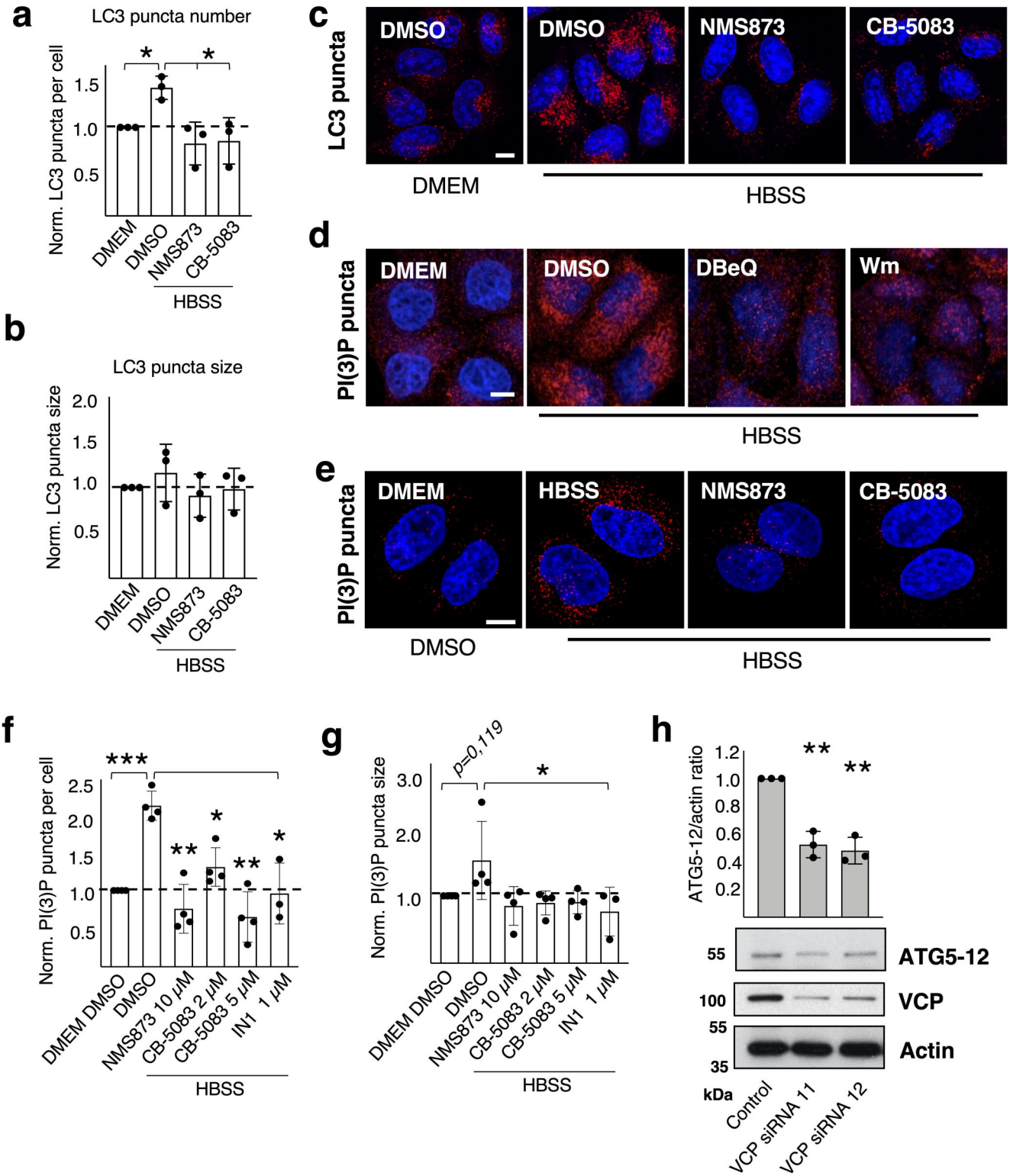

Extended Data Figure 3. Knockdown of *VCP* affects autophagy initiation

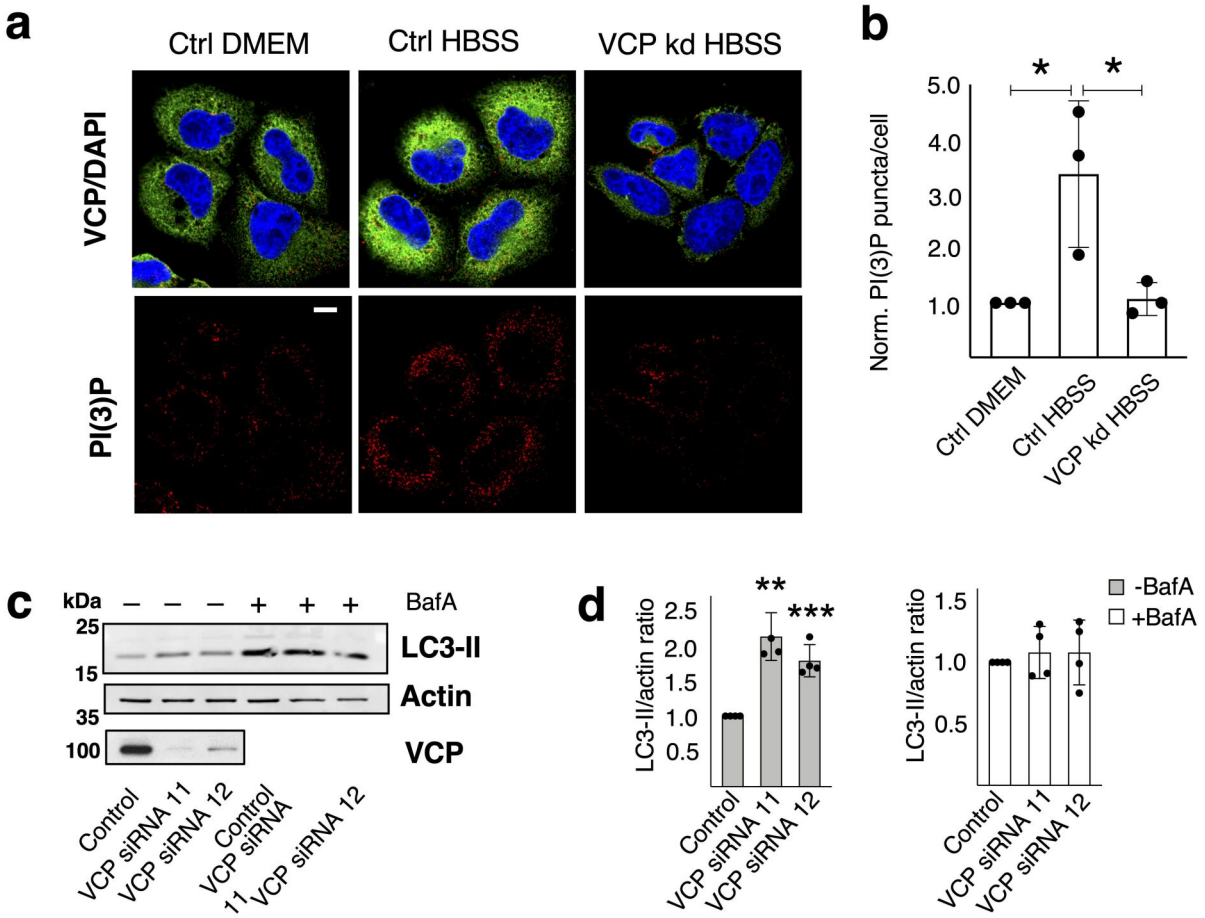

Extended Data Figure 4. VCP regulates the recruitment of early autophagy markers during starvation and mTOR inhibition

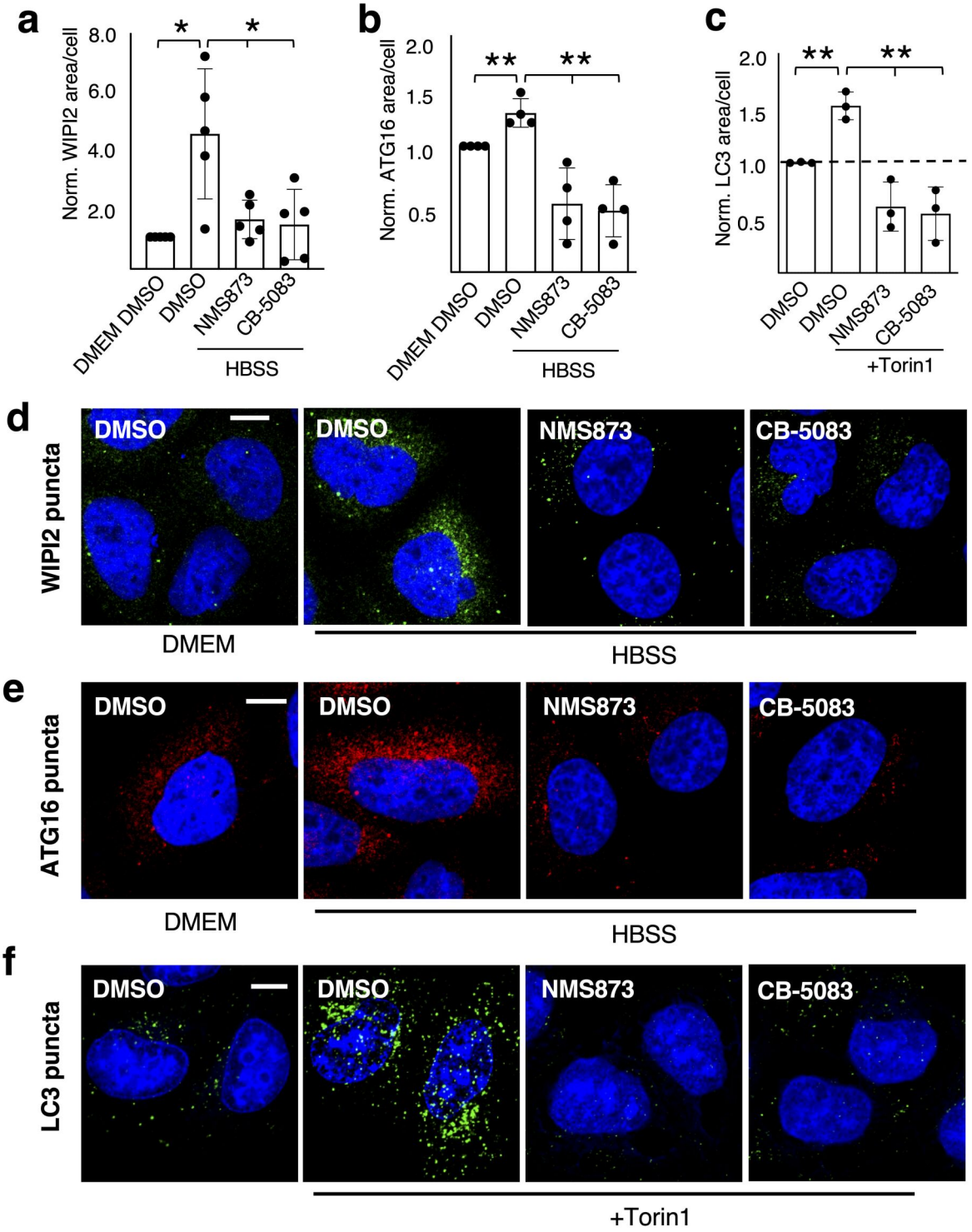

Extended Data Figure 5. VCP regulates levels of Beclin-1 and Ataxin-3

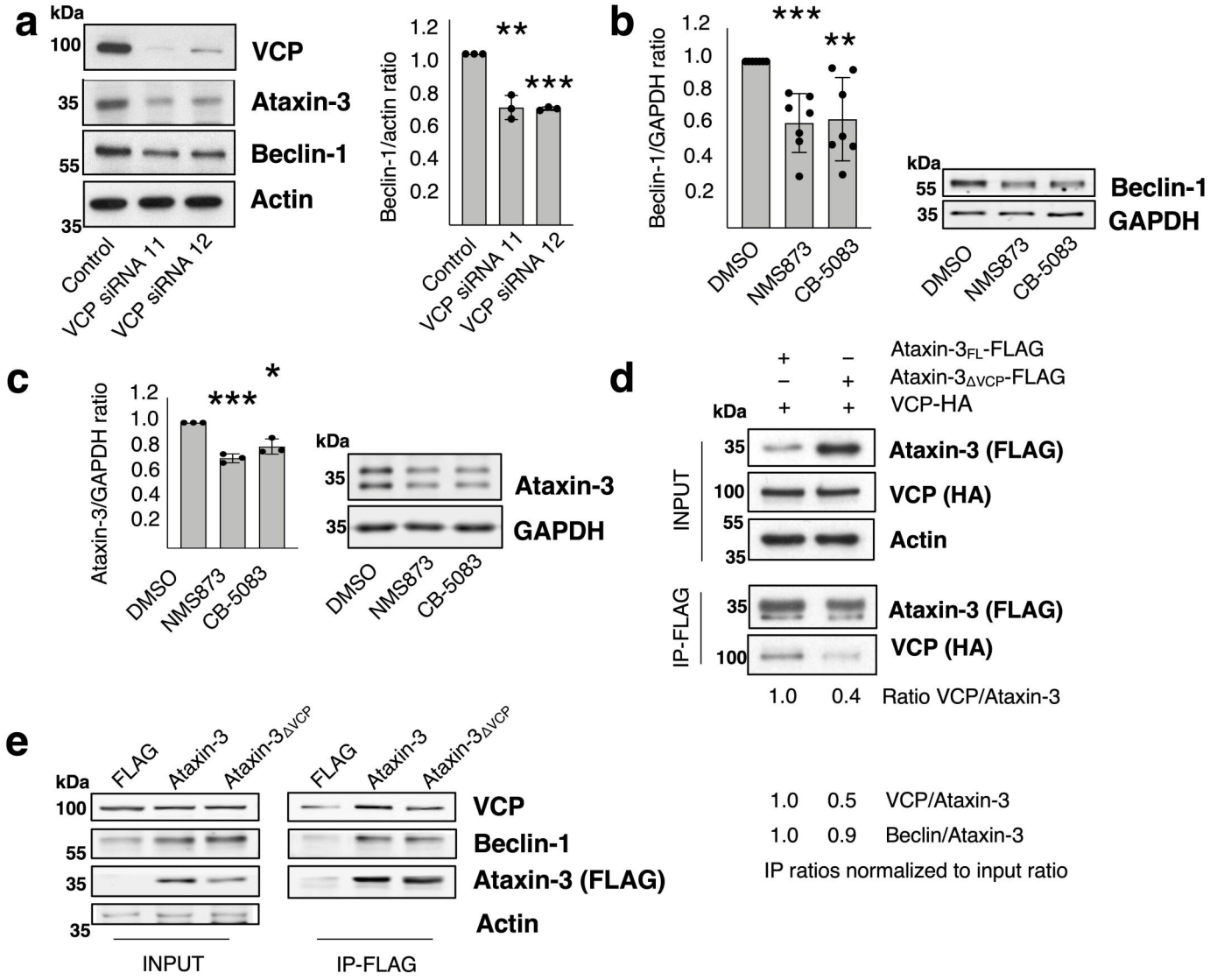

Extended Data Figure 6. VCP regulates Ataxin-3 deubiquitinase activity towards Beclin-1

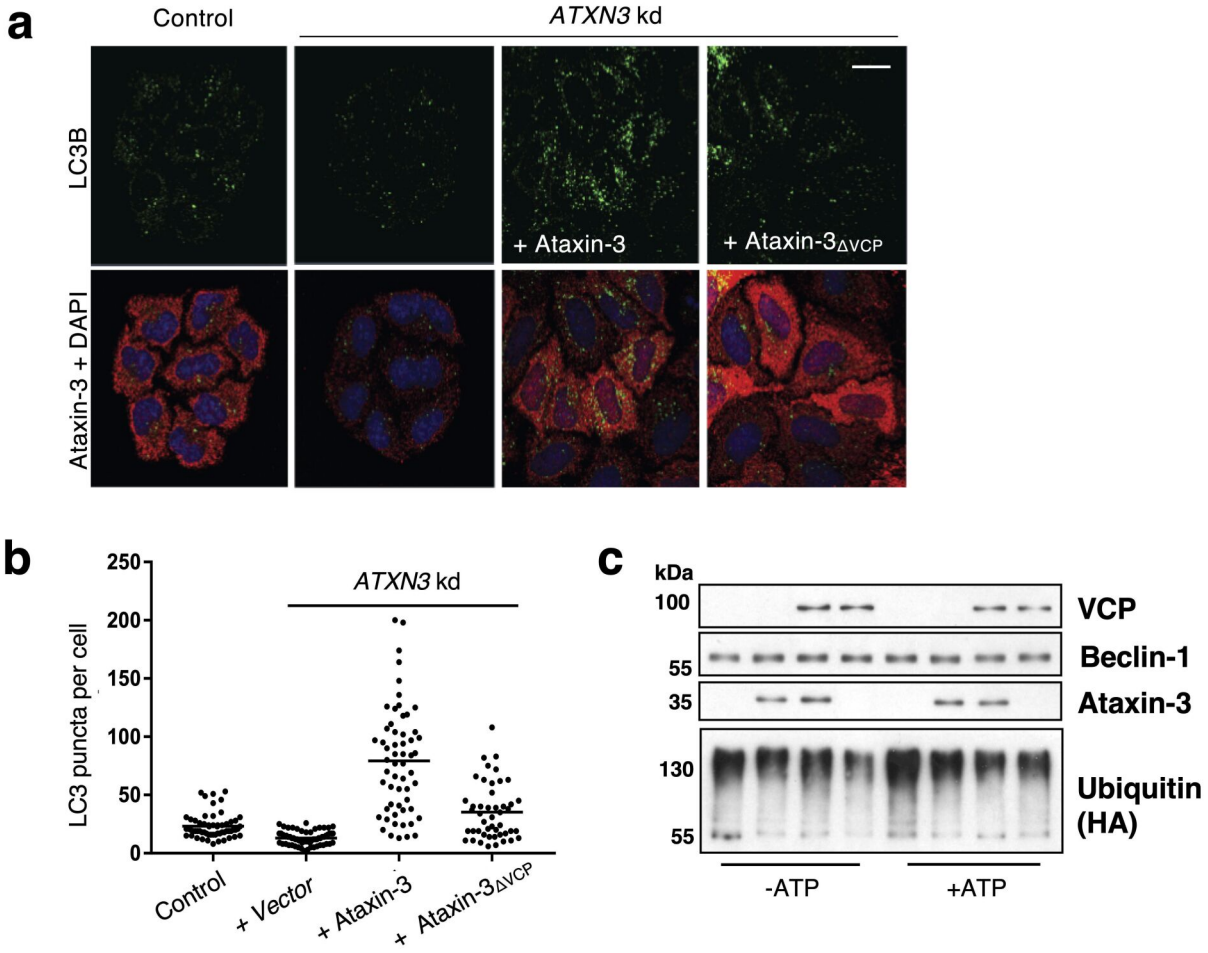

Extended Data Figure 7. VCP interacts with PI3K components *in vitro*

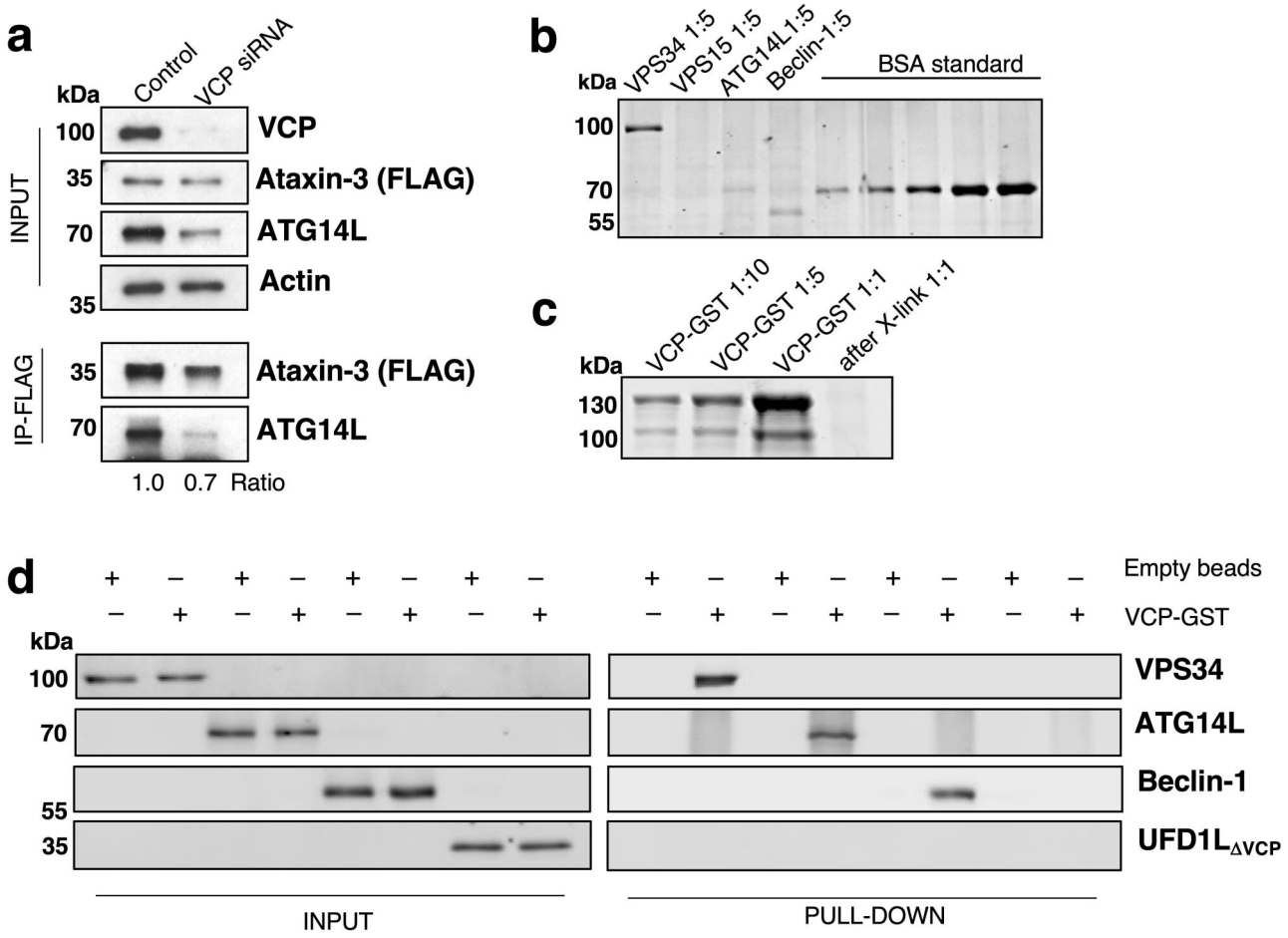

Extended Data Figure 8. VCP interacts with PI3K complex I

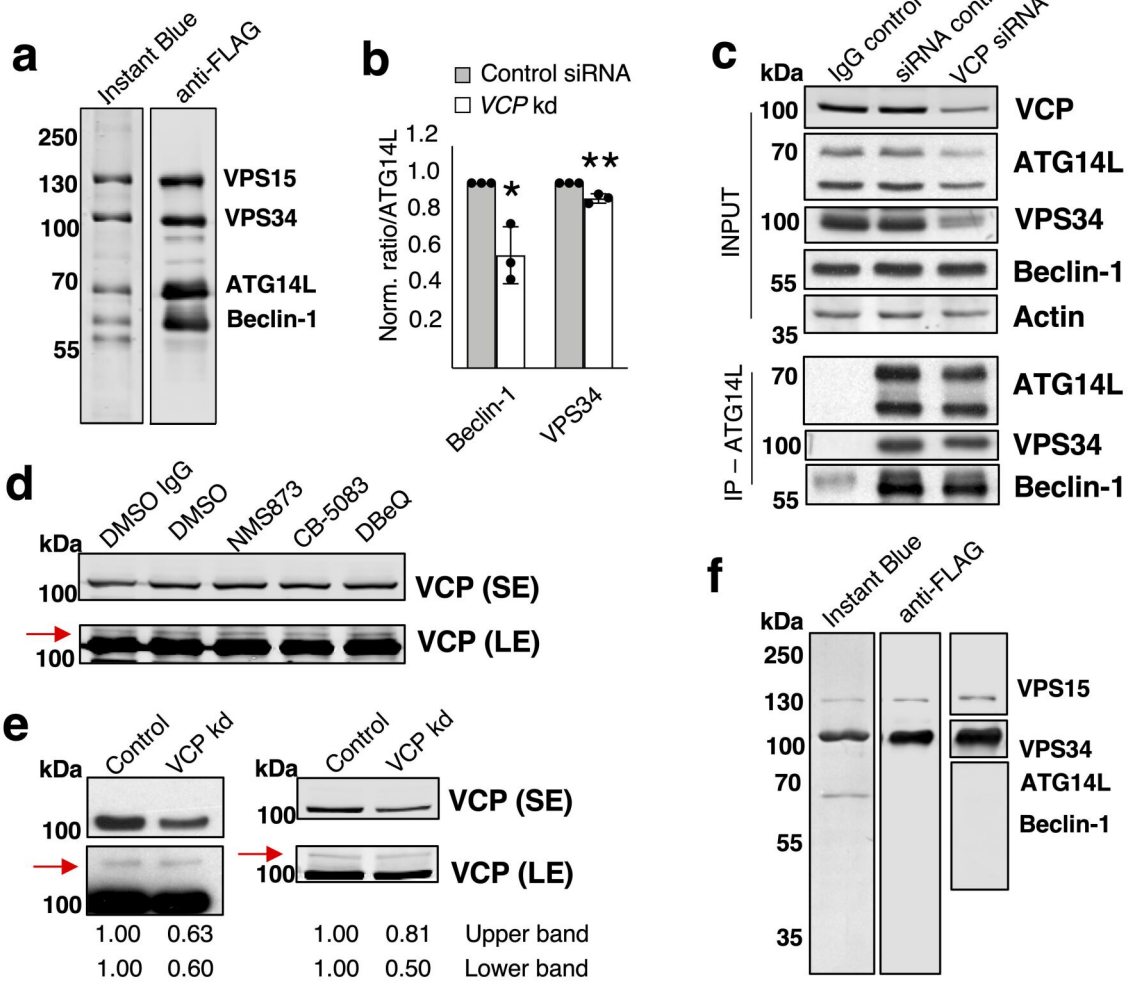

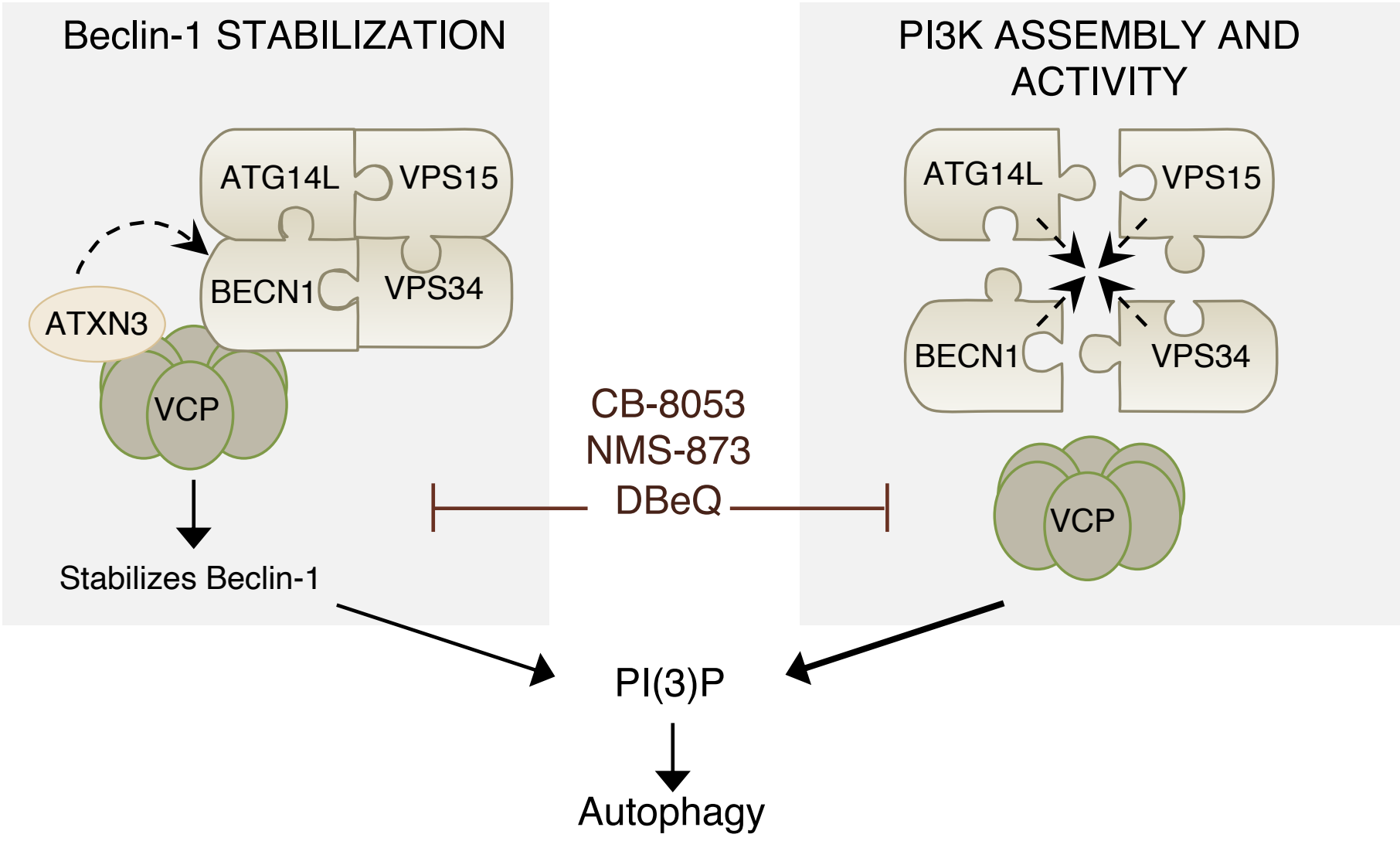
Beclin-1 STABILIZATION
ATG14L
VPS15
BECN1
VPS34
ATXN3
VCP
Stabilizes Beclin-1
CB-8053
NMS-873
DBeQ
PI3K ASSEMBLY AND ACTIVITY
ATG14L
VPS15
BECN1
VPS34
VCP
PI(3)P
Autophagy